Supporting Information for

Hollow and Highly Diastereoselective Face-Rotating Polyhedra Constructed through Rationally Engineered Facial Units

Xiao Tang[a], Zhihao Li[a], Haoliang Liu[a], Hang Qu[a], Wenbin Gao[a], Xue Dong[a], Shilin Zhang[a], Xinchang Wang[*, b], Andrew C. -H. Sue[*, a], Liulin Yang[a], Kai Tan[*, a], Zhongqun Tian[a], and Xiaoyu Cao[*, a]

[a]*State Key Laboratory of Physical Chemistry of Solid Surfaces, Key Laboratory of Chemical Biology of Fujian Province, Collaborative Innovation Center of Chemistry for Energy and Materials (iChEM) and College of Chemistry and Chemical Engineering, Xiamen University, Xiamen 361005, China.*
[b]*School of Electronic Science and Engineering, Xiamen University, Xiamen 361005, P. R. China*
[*]*E-mail: xcwang@xmu.edu.cn; andrewsue@xmu.edu.cn; ktan@xmu.edu.cn; xcao@xmu.edu.cn*

Contents

1 Instruments and materials

General. All of the chemicals, reagents, and solvents from commercial sources were used as received without further purification unless otherwise noted. Anhydrous tetrahydrofuran (THF), dichloromethane (DCM), and diethyl ether (Et_2O) were obtained by distillation over sodium or CaH_2. Column chromatography was carried out on silica gel (200 - 300 mesh). ^1H and ^{13}C nuclear magnetic resonance (NMR) spectra were recorded on a Bruker AVIII-500 spectrometer (500 MHz and 125 MHz, respectively) or Bruker AVIII-850 spectrometer at 298 K (850 MHz and 213 MHz, respectively). The spectra were referenced to residual proton-solvent references (^1H: $CDCl_3$: 7.26 ppm, benzene-d_6: 7.16 ppm; ^{13}C: $CDCl_3$: 77.16 ppm, benzene-d_6: 128.06 ppm). High-resolution mass spectra (HRMS) were recorded on a Bruker En Apex Ultra 7.0T FTMS mass spectrometer. High-performance liquid chromatography (HPLC) analysis were performed on a Shimadzu LC-16A instrument, using Daicel Chiralcel IE Columns. Circular dichroism (CD) spectra were recorded on JASCO J-810 circular dichroism spectrometer at 298 K. All CD spectra of the separated enantiomers were measured in toluene. Single crystal X-ray diffraction data were collected on Rigaku SuperNova X-Ray single crystal diffractometer using Cu Kα (λ = 1.54184 Å) micro-focus X-ray sources at 100 K.

A list of abbreviations:

CD: circular dichroism
COSY: correlation spectroscopy
DCM: dichloromethane
DEPT: distortionless enhancement by polarization transfer
DMF: N,N-dimethylformamide
DMSO: dimethyl sulfoxide
EA: ester acetate
HMBC: ^1H detected heteronuclear multiple bond correlation
HPLC: high-performance liquid chromatography
HSQC: heteronuclear single-quantum correlation
NMR: nuclear magnetic resonance
NOESY: nuclear overhauser enhancement spectroscopy
PE: petrol ether
rt: room temperature
THF: tetrahydrofuran

2 Experimental section

Synthesis processes of building blocks.

TAT-m[1]:

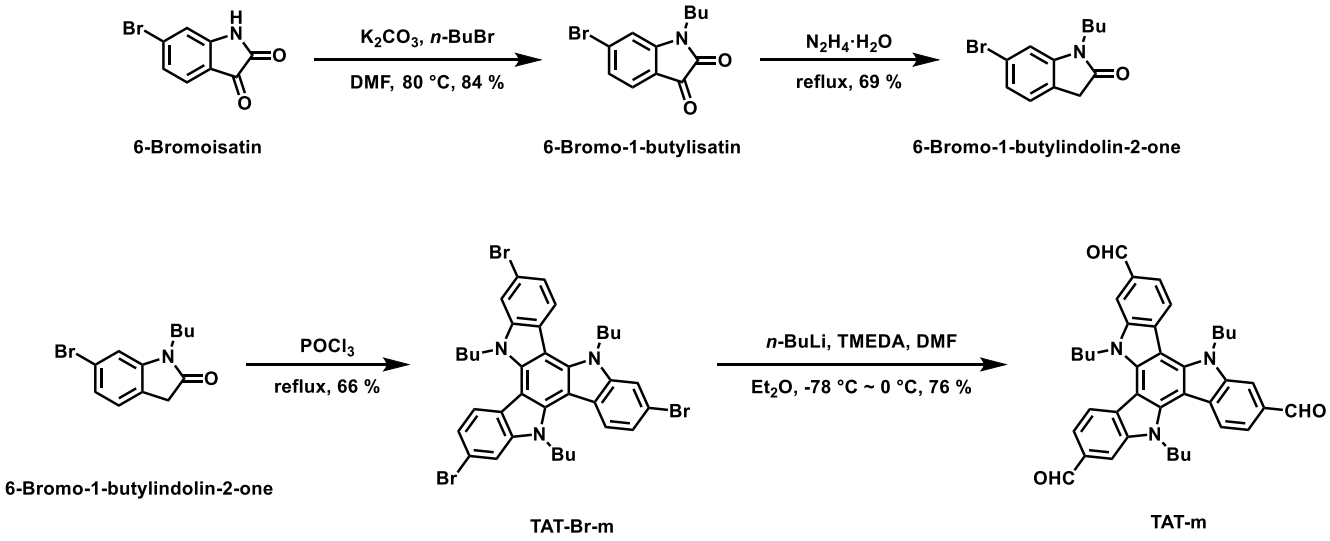

Figure S1 | Synthesis processes of **TAT-m**.

6-Bromo-1-butylisatin. **6-Bromoisatin** (22.6 g, 100 mmol) and K_2CO_3 were dispersed in DMF (300 mL) and stirred at 60 °C for 2 h. Bromobutane (13 mL, 120 mmol) was added and the reaction was warmed to 80 °C and stirred for 15 h. Water (300 mL) was added to quench the reaction and afforded crude product as brown solid. The crude product was washed by water (300 mL) for three times and dried under vacuum to give pure **6-Bromo-1-butylisatin** (23.7 g, 84 %). ^{1}H NMR (500 MHz, $CDCl_3$) δ 7.45 (d, J = 7.9 Hz, 1H), 7.28 (dd, J = 7.9 Hz, 1.4 Hz, 1H), 7.06 (d, J = 1.4 Hz, 1H), 3.70 (t, J = 7.4 Hz, 2H), 1.72–1.64 (m, 2H), 1.44–1.38 (m, 2H), 0.98 (t, J = 7.4 Hz, 3H).

6-Bromo-1-butylindolin-2-one. **6-Bromo-1-butylisatin** (19.8 g, 70 mmol) was added to hydrazine hydrate (85 %, 50 mL), and the mixture was stirred at 120 °C for 5 h. The reaction was quenched by 50 % HCl and extracted by DCM. The combined organic phase was dried over Na_2SO_4, and evaporated under vacuum. The crude product was purified by column chromatography with DCM to give pure **6-Bromo-1-butylindolin-2-one** as white solid (12.9 g, 69 %). ^{1}H NMR (500 MHz, $CDCl_3$) δ 7.15 (dd, J = 7.8, 1.6 Hz, 1H), 7.09 (d, J = 7.8 Hz, 1H), 6.96 (s, 1H), 3.67 (t, J = 7.4 Hz, 2H), 3.45 (s, 2H), 1.69–1.60 (m, 2H), 1.43–1.35 (m, 2H), 0.96 (t, J = 7.4 Hz, 3H).

TAT-Br-m. Under N_2, $POCl_3$ (50 mL) was added to **6-Bromo-1-butylindolin-2-one** (2.67 g, 10 mmol). The reaction was stirred at 110 °C for 4 h and then quenched by ice water (300 mL) carefully. The mixture was extracted by DCM and dried over Na_2SO_4, the crude product was purified by column chromatography with DCM/PE (v/v = 1/4) to give **TAT-Br-m** as white solid (1.6 g, 66 %). ^{1}H NMR (500

MHz, $CDCl_3$) δ 8.01 (d, J = 8.6 Hz, 3H), 7.70 (d, J = 1.3 Hz, 3H), 7.42 (dd, J = 8.6, 1.5 Hz, 3H), 4.73 (t, J = 7.4 Hz, 6H), 1.89–1.83 (m, 6H), 1.23–1.20 (m, 6H), 0.85 (t, J = 7.4 Hz, 9H).

TAT-m. **TAT-Br-m** (1 g, 1.37 mmol) was dissolved in anhydrous Et_2O (80 mL) and cooled to -78 °C under N_2. Then *n*-BuLi (17.1 mL, 41.1 mmol, 2.4 M in Hexane) and tetramethylethylenediamine (**TMEDA**, 6.2 mL, 41.1 mmol) were added dropwise. And the mixture was stirred for 30 min at -78 °C, then warm to 0 °C for 30 min and to room temperature for another 30 min. After that, the mixture was cooled to -78 °C, followed by slow addition of anhydrous DMF (3.9 mL, 50 mmol) and overnight stirring at that temperature. Then the reaction mixture was warmed to room temperature and quenched by hydrochloric acid (2 M, 150 mL). The mixture was extracted by DCM and dried over Na_2SO_4. The solvent was removed by evaporated in vacuum, and the crude product was purified by recrystalization with toluene to give pure **TAT-m** as yellow powder (622 mg, 76 %). ^{1}H NMR (500 MHz, $CDCl_3$) δ 10.21 (s, 3H), 8.35 (d, J = 8.3 Hz, 3H), 8.18 (s, 3H), 7.90 (dd, J = 8.3, 0.9 Hz, 3H), 5.00 (t, J = 7.4 Hz, 6H), 2.00–1.94 (m, 6H), 1.31–1.25 (m, 6H), 0.87 (t, J = 7.4 Hz, 9H). ^{13}C NMR (126 MHz, $CDCl_3$) δ 192.43, 142.06, 140.90, 132.01, 128.49, 123.24, 121.86, 112.41, 103.73, 47.67, 32.44, 20.36, 14.14.

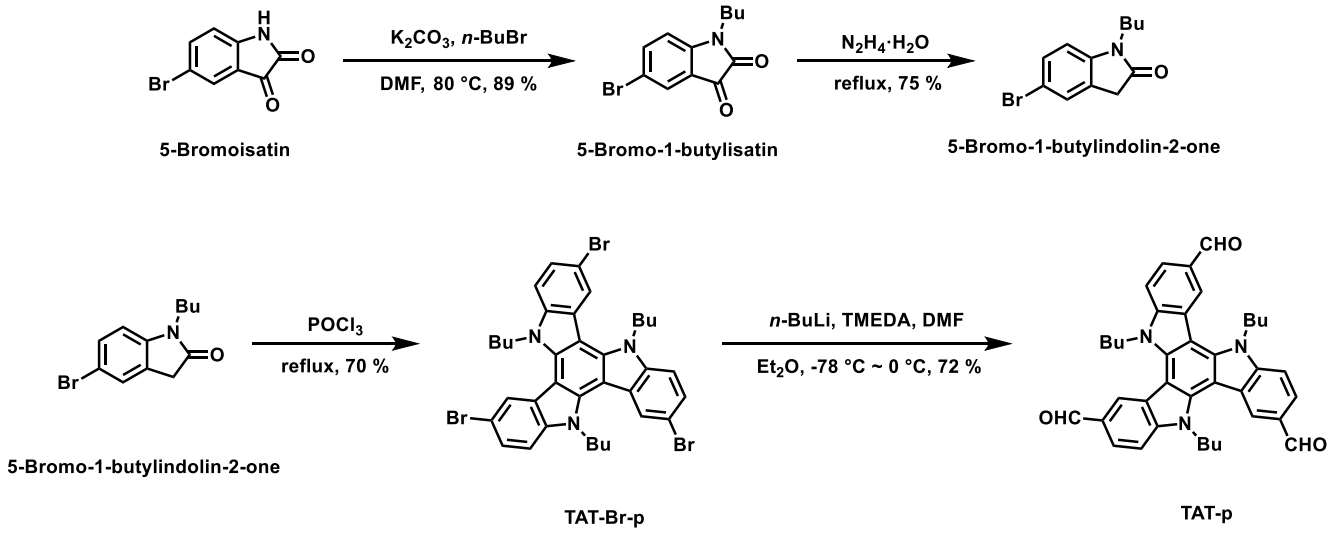

Figure S2 | **TAT-p** was synthesized through the same method as **TAT-m**.

TAT-p was synthesized through the same method as **TAT-m** by changing the starting material from **6-Bromoisatin** to **5-Bromoisatin**.

TAT-Br-p. ^{1}H NMR (500 MHz, $CDCl_3$) δ 8.25 (d, J = 1.6 Hz, 3H), 7.53 (dd, J = 8.6, 1.7 Hz, 3H), 7.45 (d, J = 8.6 Hz, 3H), 4.70 (t, J = 7.4 Hz, 6H), 2.00–1.93 (m, 6H), 1.36–1.33 (m, 6H), 0.93 (t, J = 7.4 Hz, 9H).

TAT-p. ^{1}H NMR (500 MHz, $CDCl_3$) δ 10.18 (s, 3H), 8.80 (s, 3H), 8.02 (d, J = 8.3 Hz, 3H), 7.74 (d, J = 8.4 Hz, 3H), 4.97 (t, J = 7.4 Hz, 6H), 2.12–1.99 (m, 6H), 1.42–1.39 (m, 6H), 0.93 (t, J = 7.3 Hz, 9H). ^{13}C NMR (126 MHz, $CDCl_3$) δ 189.62, 146.35, 140.51, 129.74, 127.73, 124.26, 122.80, 111.18, 105.78, 47.63, 32.66, 20.30, 14.21.

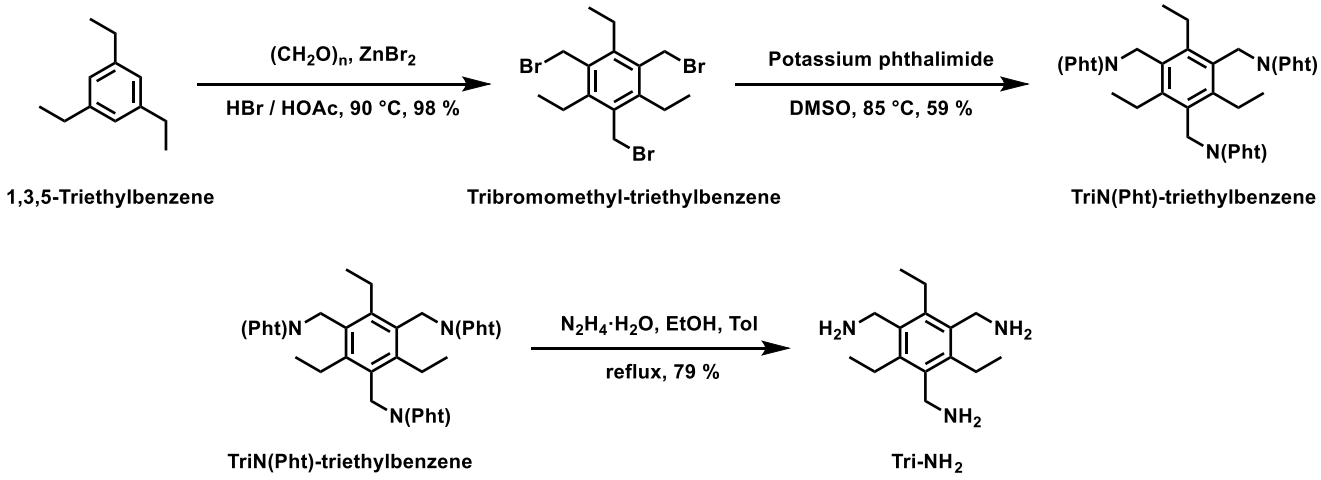

Figure S3 | **Tri-NH$_2$** was synthesized through reported method.

Tri-NH$_2$ were synthesized through reported methods[2].

FRP-**12**: Trifluoroacetic acid (TFA, 7.5 % equiv.) was added to a 40 mL toluene solution of **Tri-NH$_2$** (8.37 mg, 33.4 μmol, 1 equiv.), and **TAT-m** (20 mg, 33.4 μmol, 1 equiv., dissolved in 40 mL toluene) was added dropwised under 110 °C. The mixture was stirred at the same temperature for 48 h and then quenched by excessive K_2CO_3. The solution was filtrated and concentrated under vacuum. The crude product was purified by chiral HPLC and the yield of FRP-**12** was calculated to be 91.5%.

FRP-**13** was prepared in the same way from **TAT-p** and **Tri-NH$_2$** and the yield was calculated to be 96.7%.

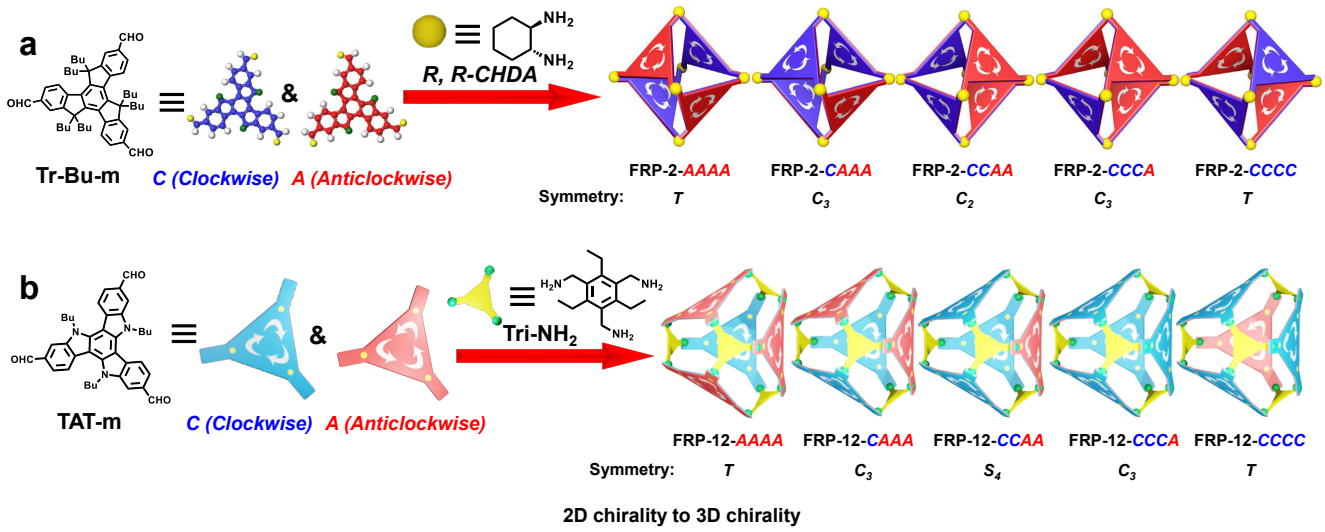

Figure S4 | The complex arrangements of rotational patterns might result in a series of possible diastereoisomers with different symmetry. (a) **Tr**-based FRP and (b) **TAT**-based FRP.

3 NMR spectra

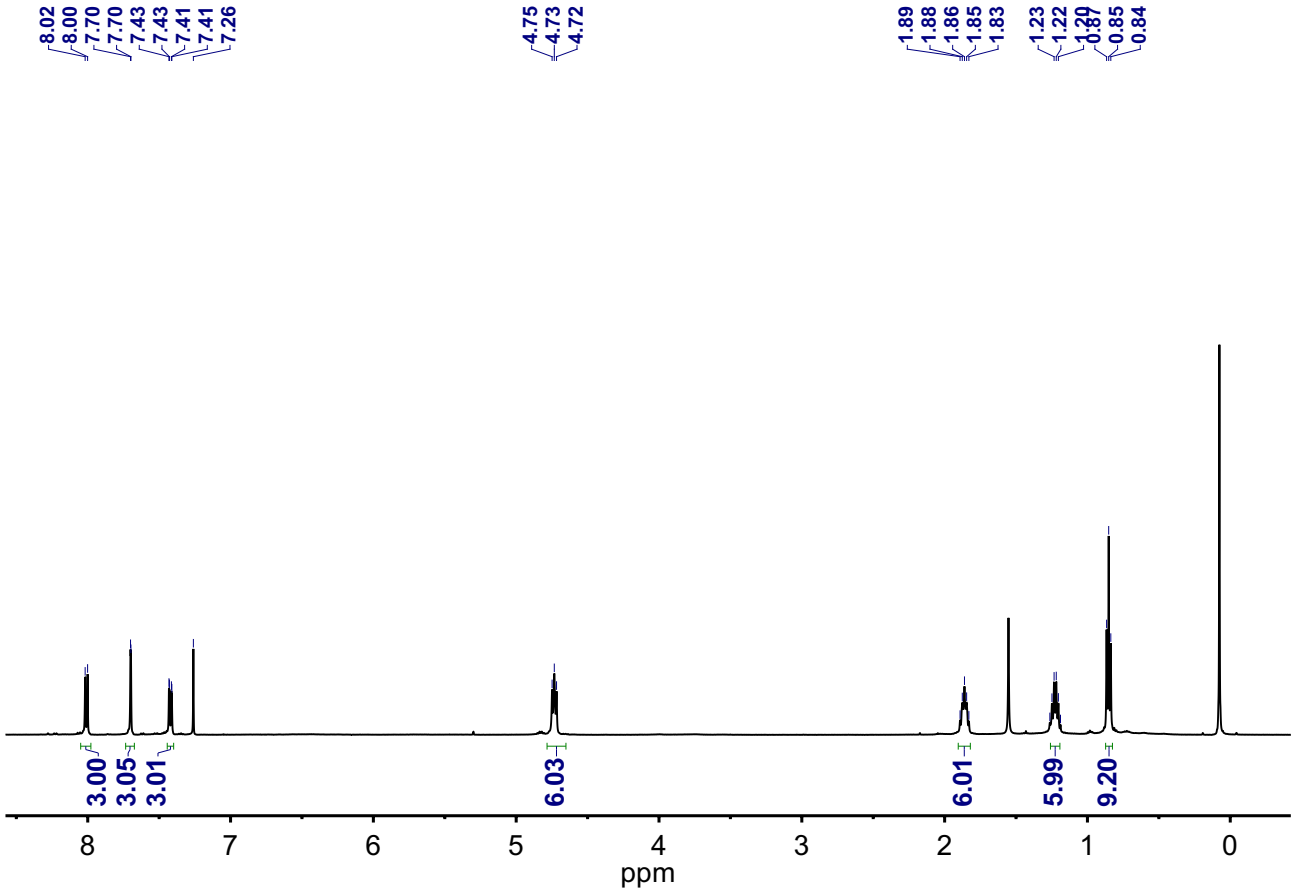

Figure S5 | ^{1}H NMR spectrum of **TAT-Br-m**.

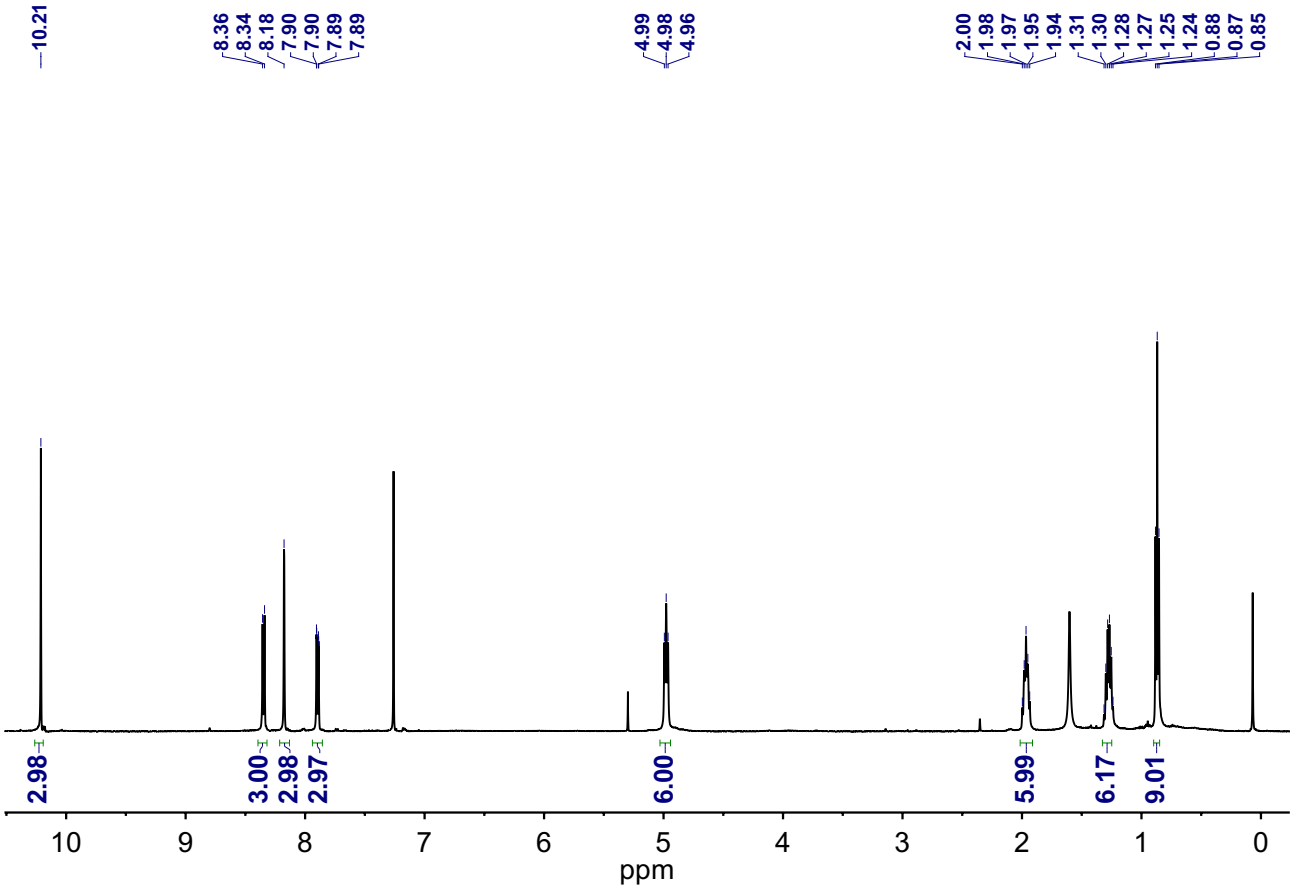

Figure S6 | ^{1}H NMR spectrum of **TAT-m**.

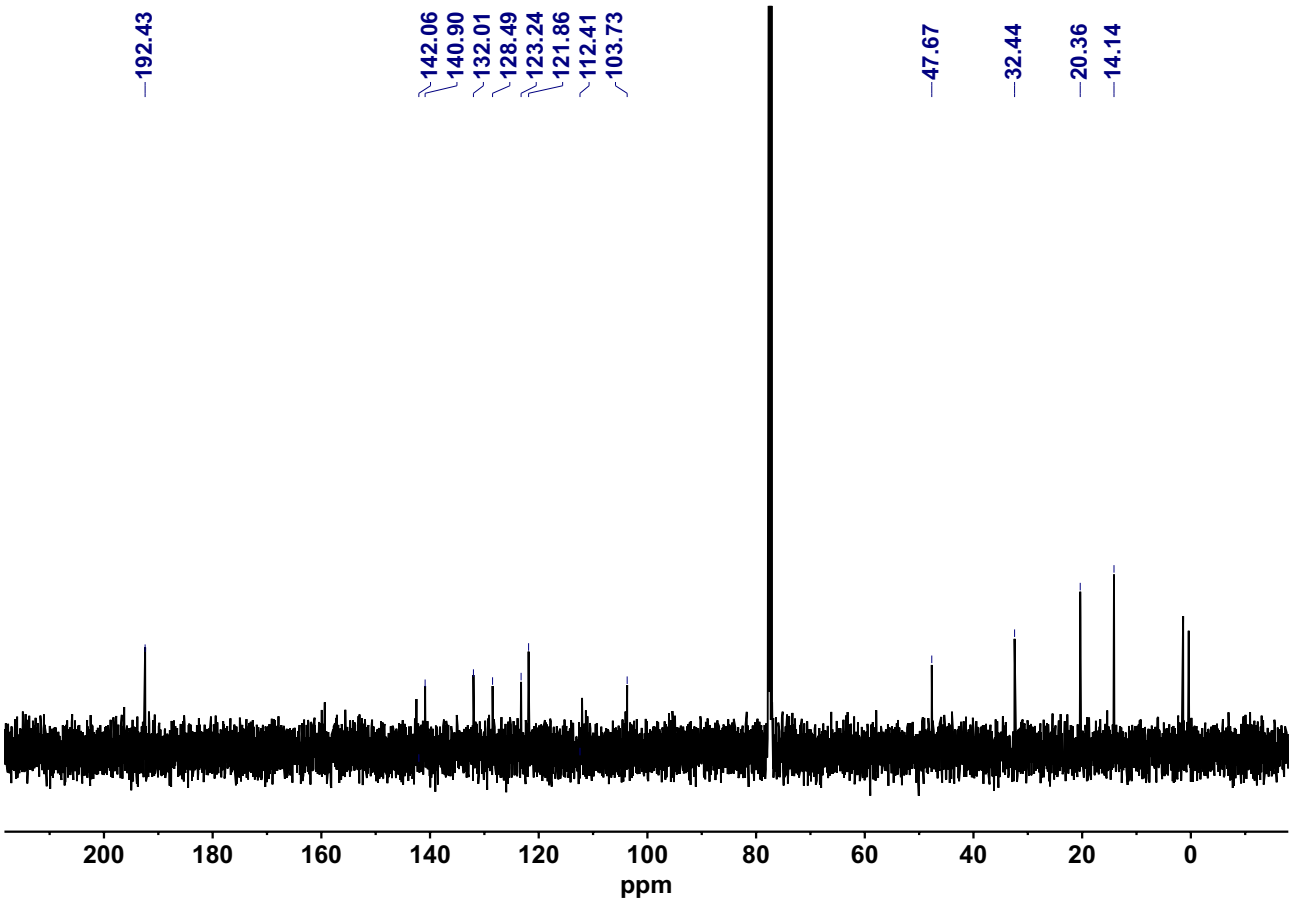

Figure S7 | ^{13}C NMR spectrum of **TAT-m**.

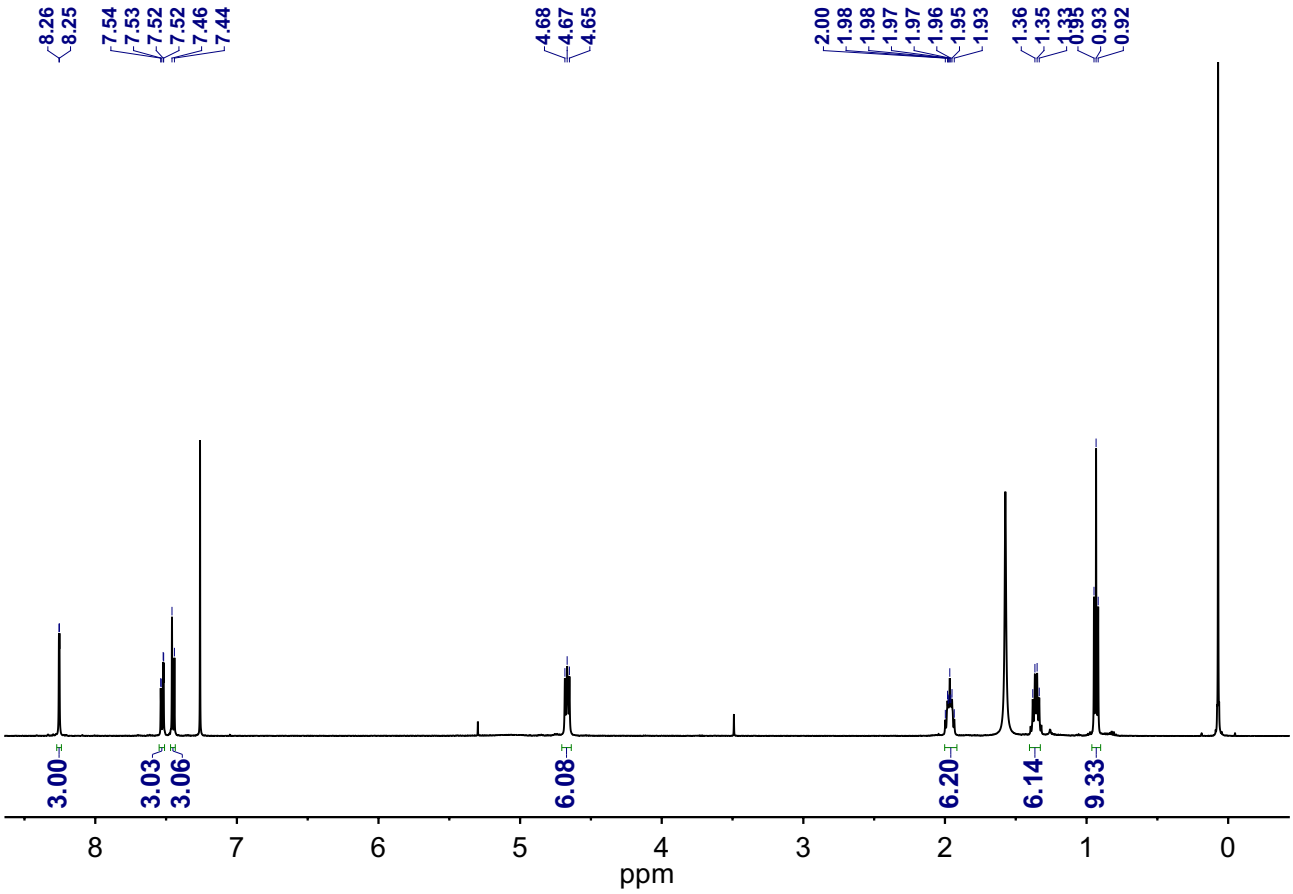

Figure S8 | ^{1}H NMR spectrum of **TAT-Br-p**.

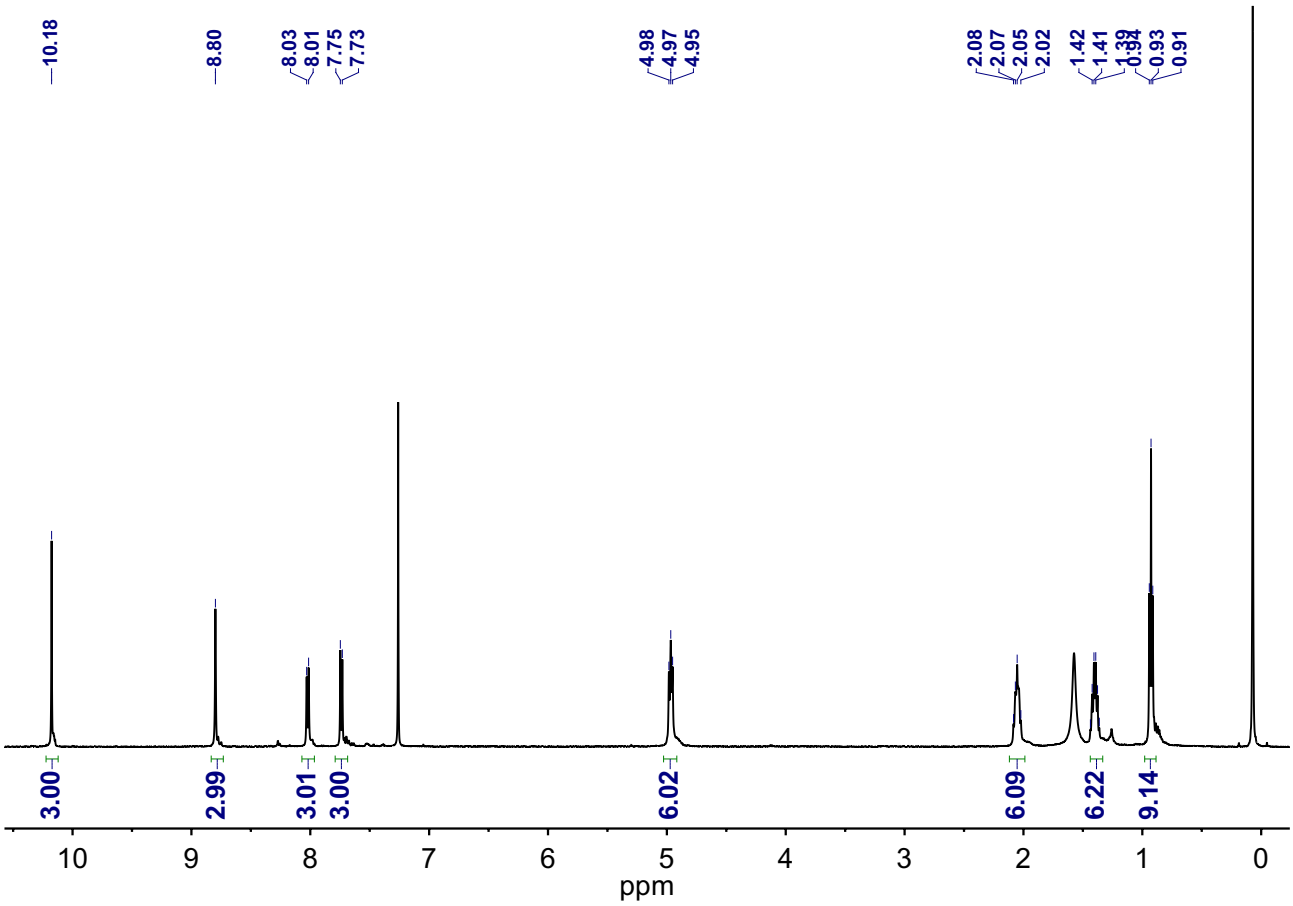

Figure S9 | ^{1}H NMR spectrum of **TAT-p**.

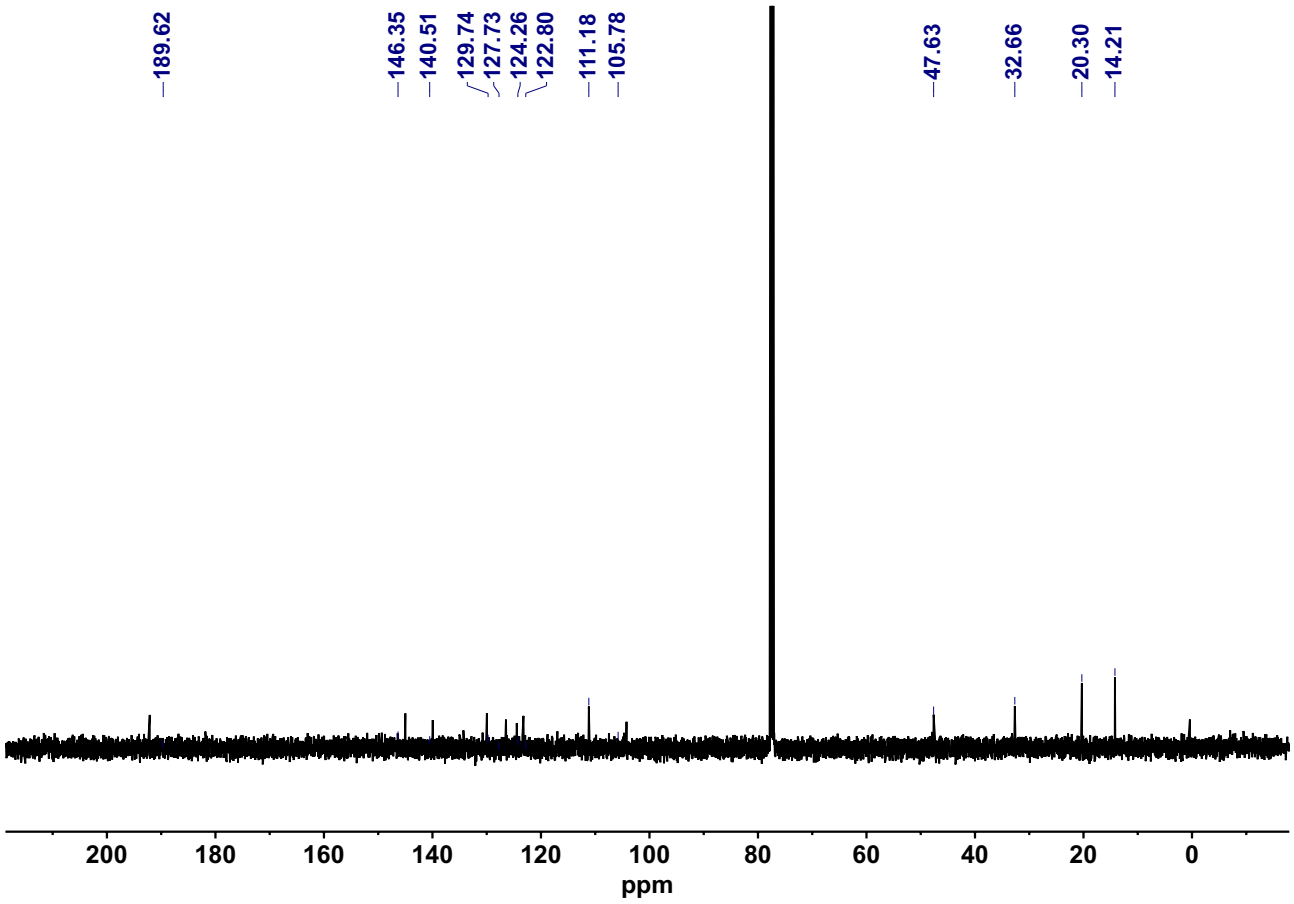

Figure S10 | ^{13}C NMR spectrum of **TAT-p**.

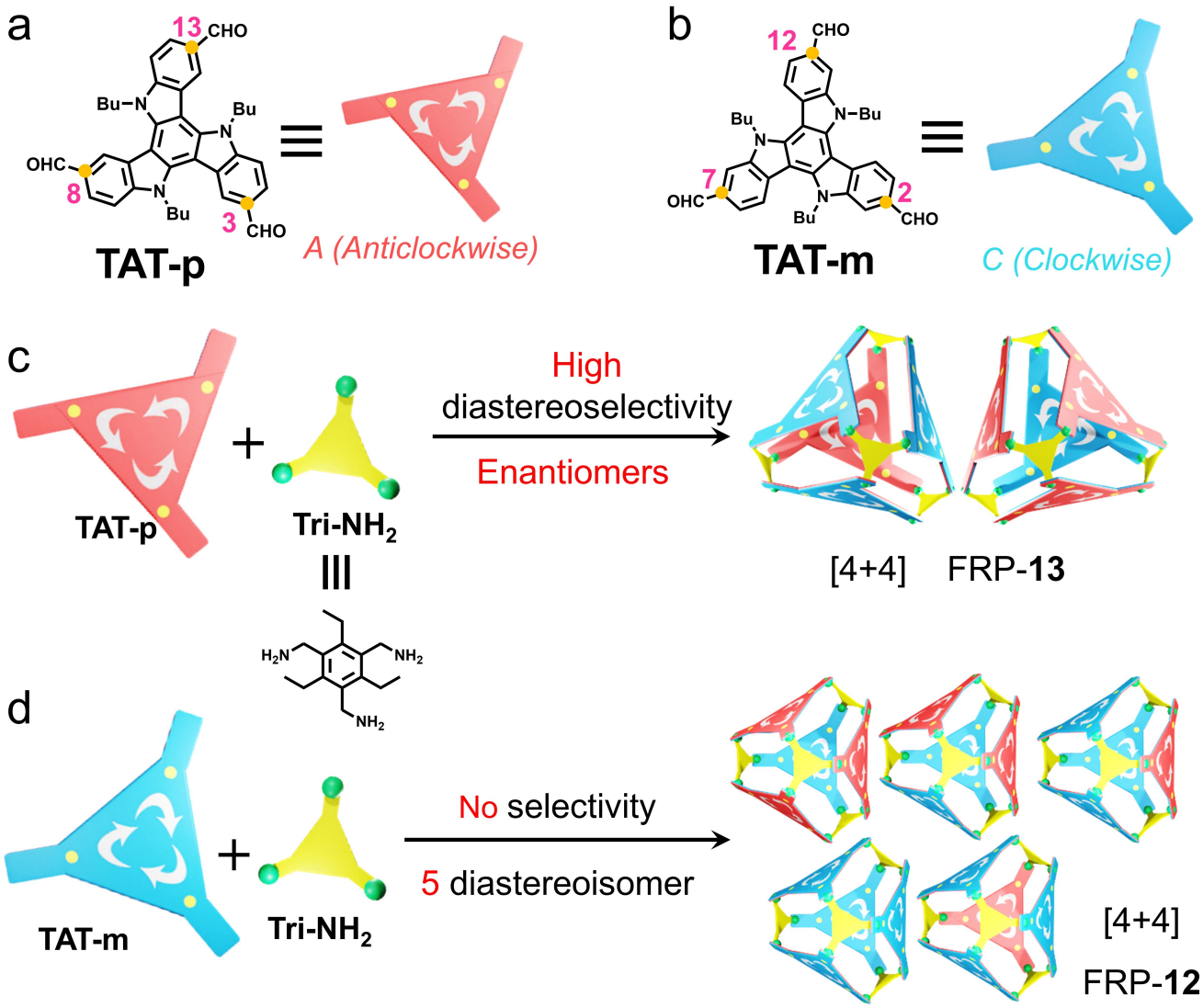

Figure S11 | FRP constructed from **TAT** units. The *para*-formyl substituted C_{3h}-symmtric facial building blocks resulted in homo-directional products and the *meta*-formyl substituted units gave five diastereoisomers.

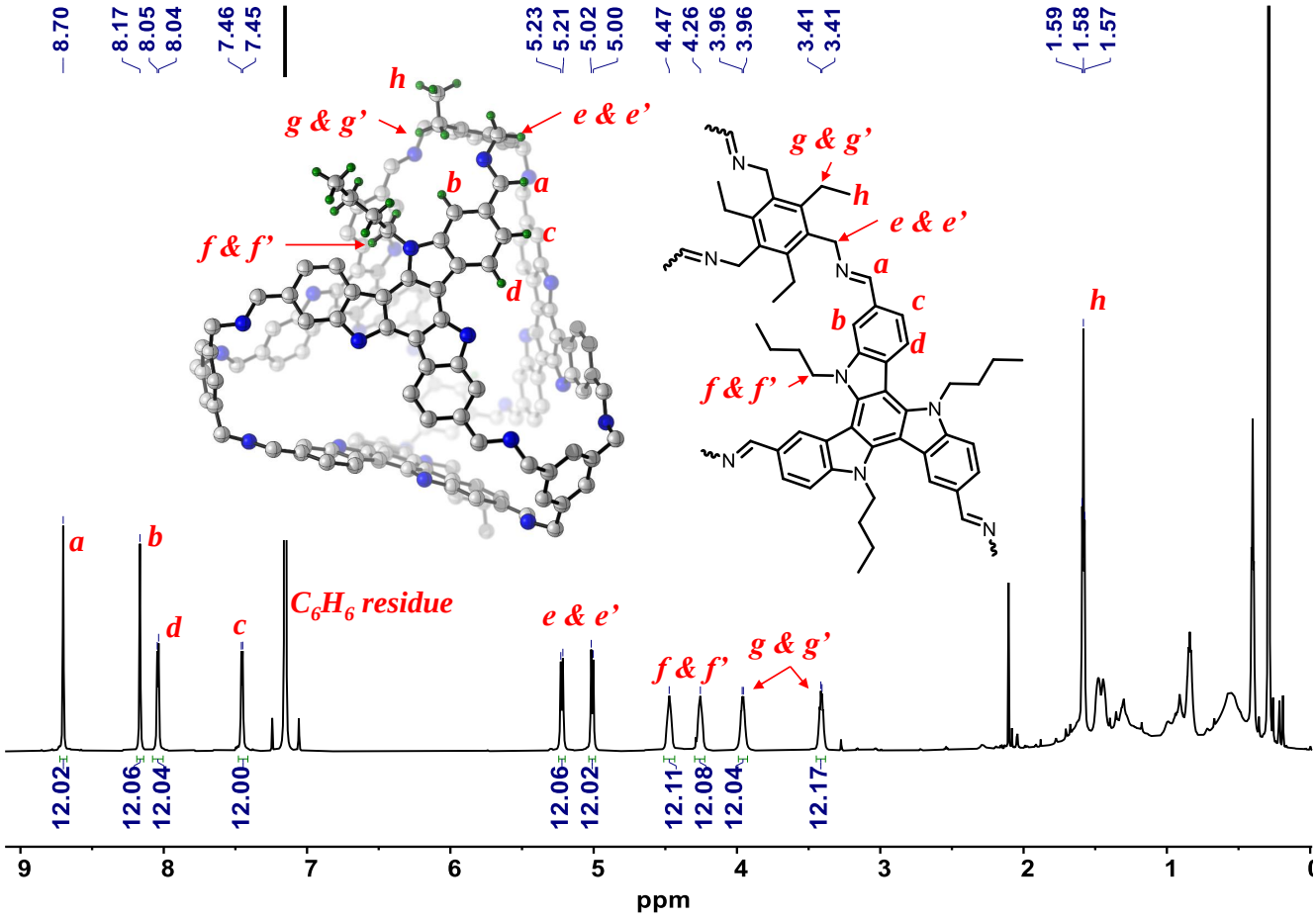

Figure S12 | ^{1}H NMR spectrum of FRP-**12**-*CCCC* and *AAAA*.

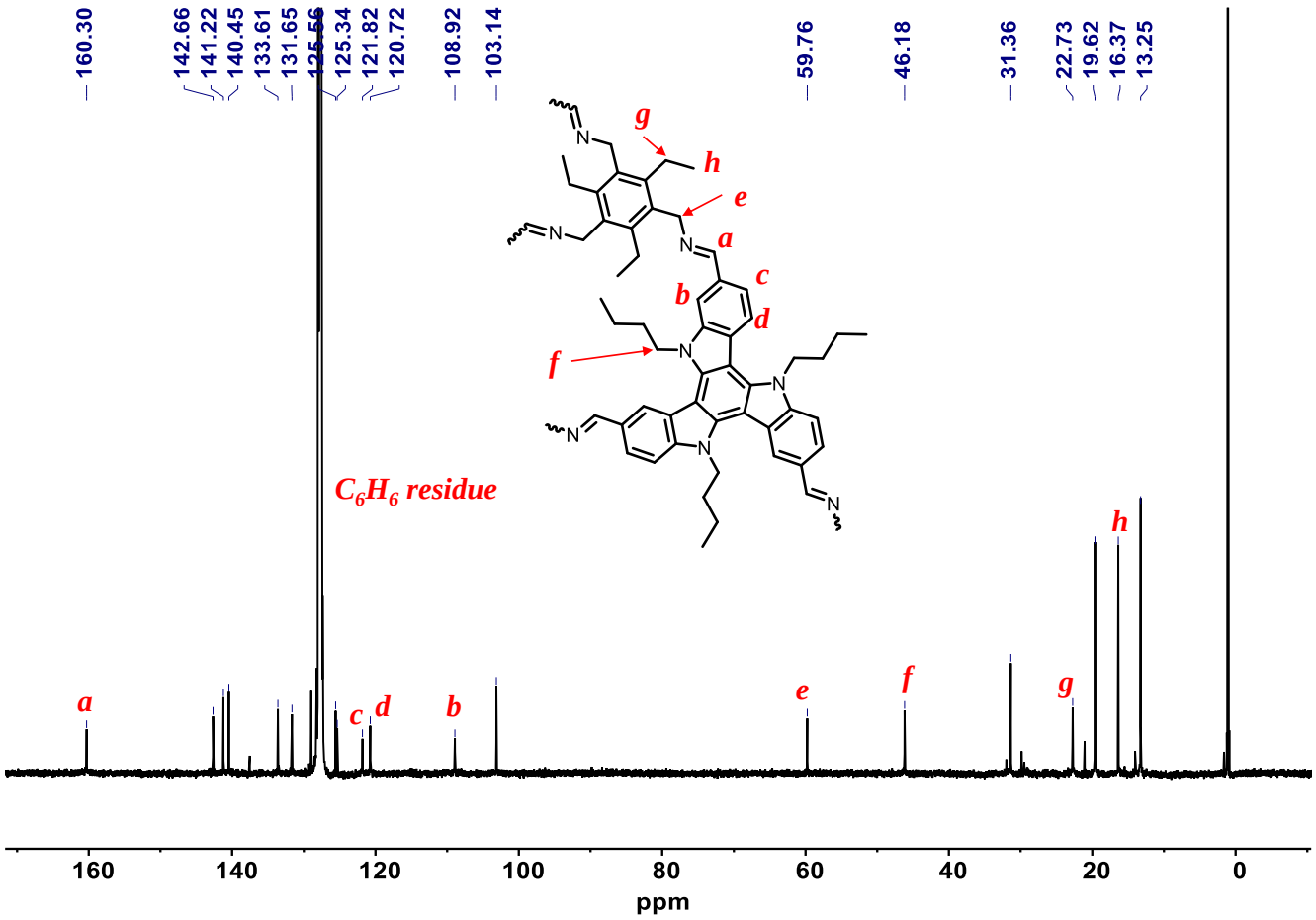

Figure S13 | ^{13}C NMR spectrum of FRP-**12**-*CCCC* and *AAAA*.

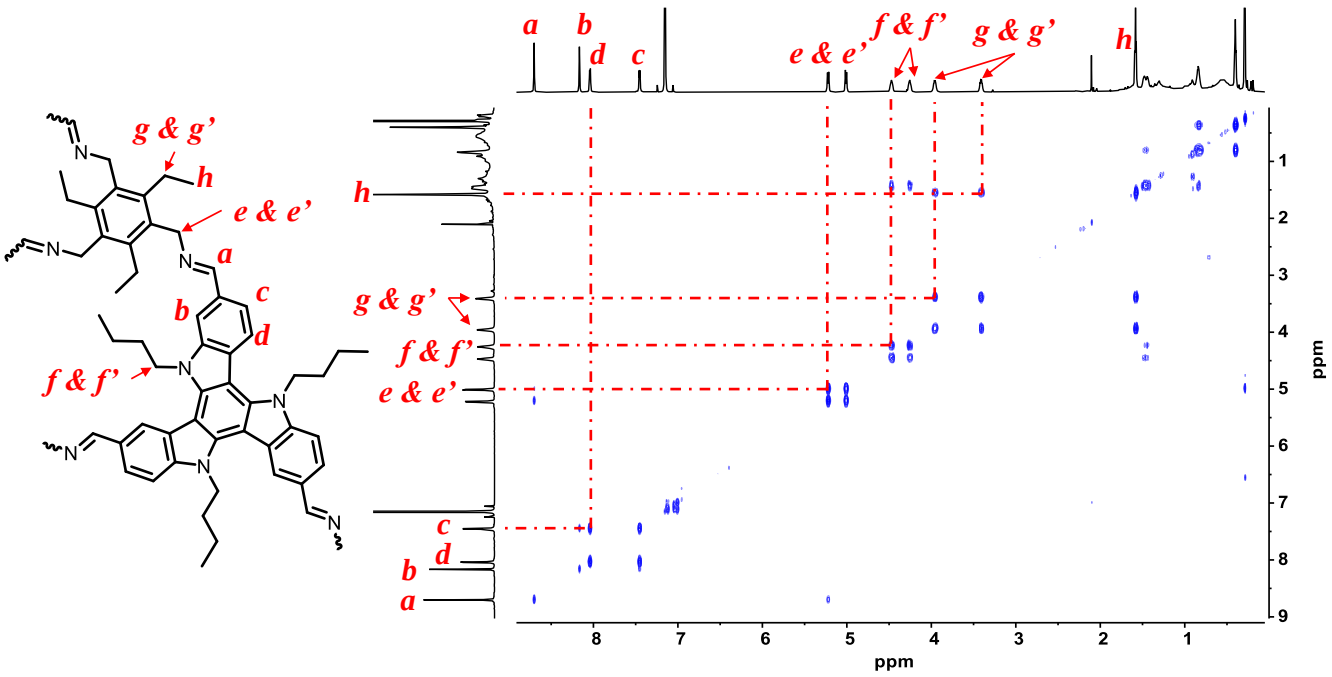

Figure S14 | H-H COSY spectrum of FRP-**12**-*CCCC* and *AAAA*.

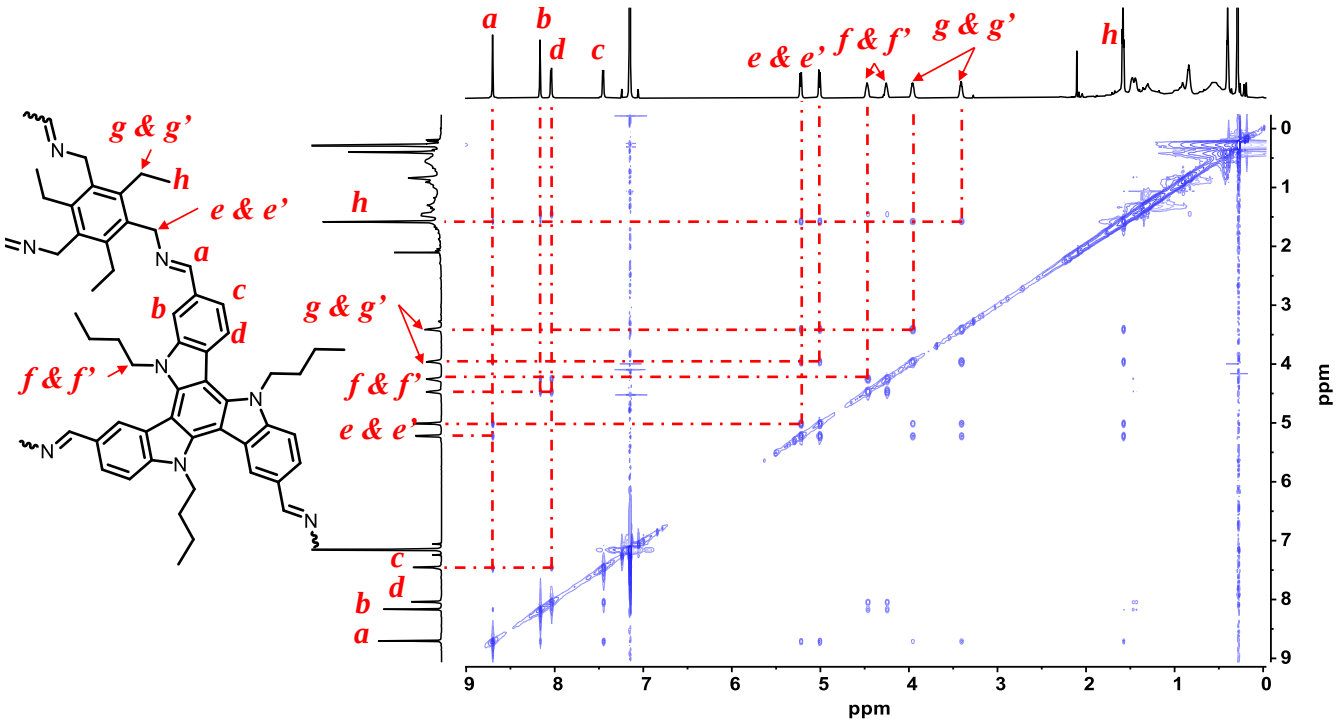

Figure S15 | NOESY spectrum of FRP-**12**-*CCCC* and *AAAA*.

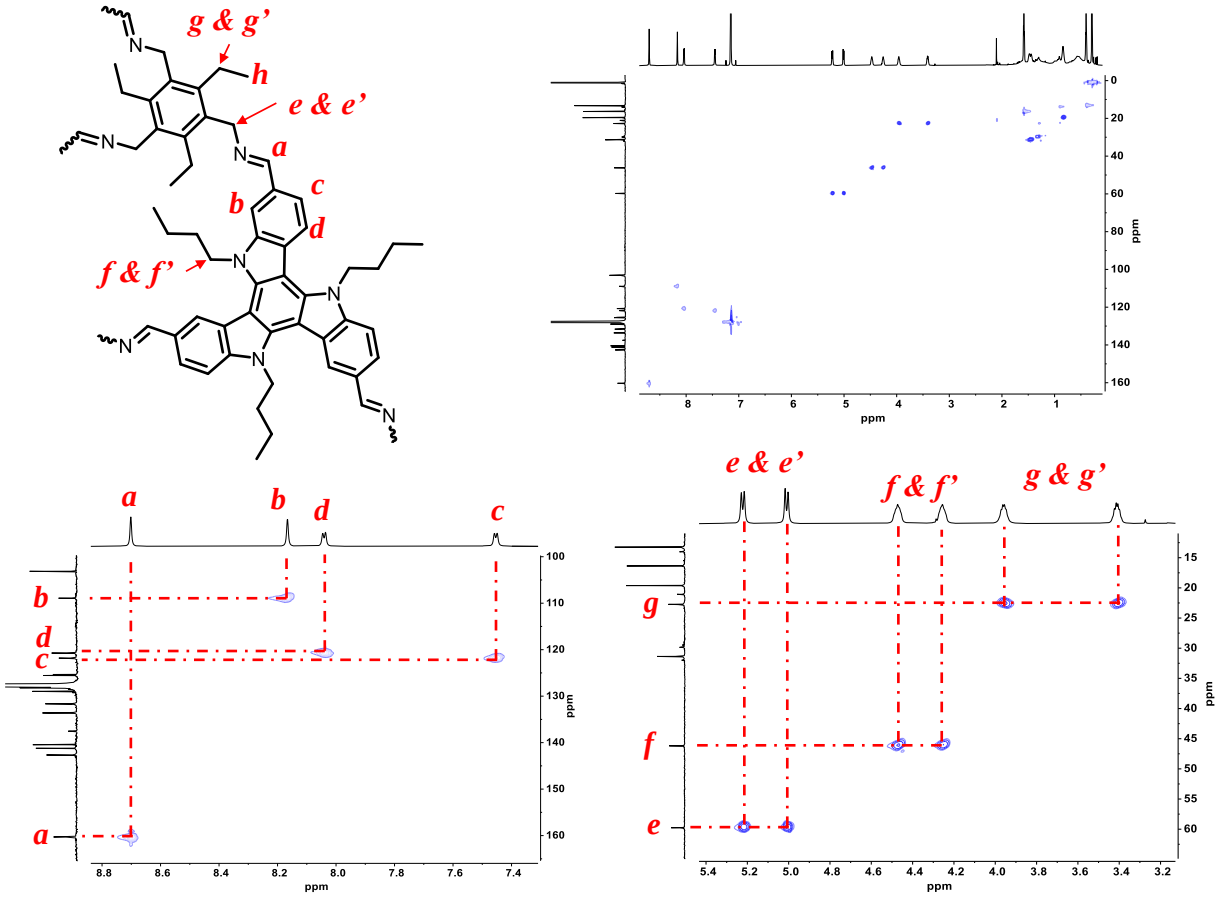

Figure S16 | HSQC spectrum of FRP-**12**-*CCCC* and *AAAA*.

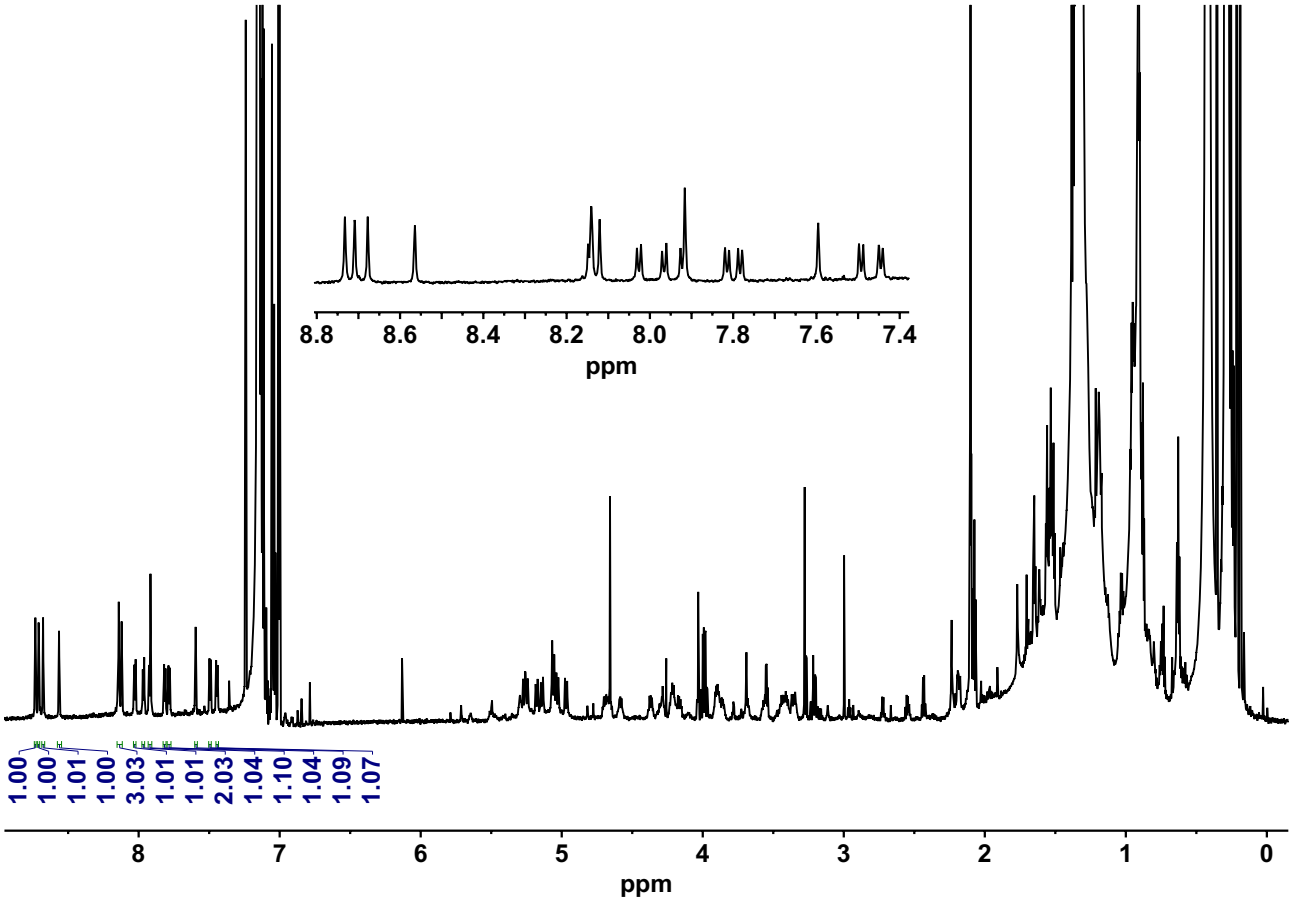

Figure S17 | ^{1}H NMR spectrum of FRP-**12**-*CCCA* and *CAAA*.

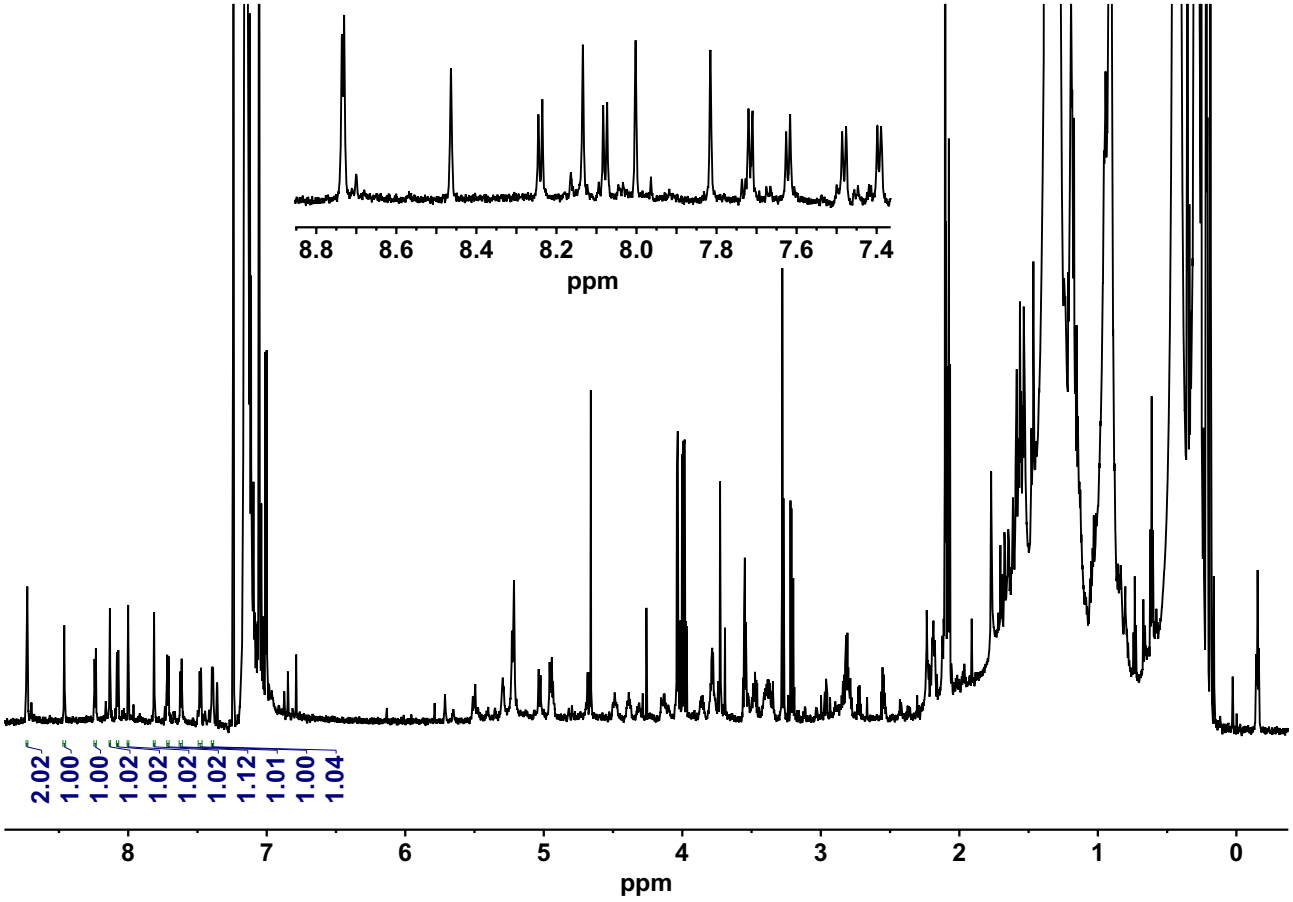

Figure S18 | ^{1}H NMR spectrum of FRP-**12**-*CCAA*. The non-trivial separation and the poor stability made it difficult to perform the NMR characterization of the hetero-directional products of FRP-**12** (*CCCA*, *CAAA* and *CCAA*). And the ^{1}H spectra shown in Figure S17 and S18 are the best ones compared to the other NMR results for hetero-directional FRP-**12**.

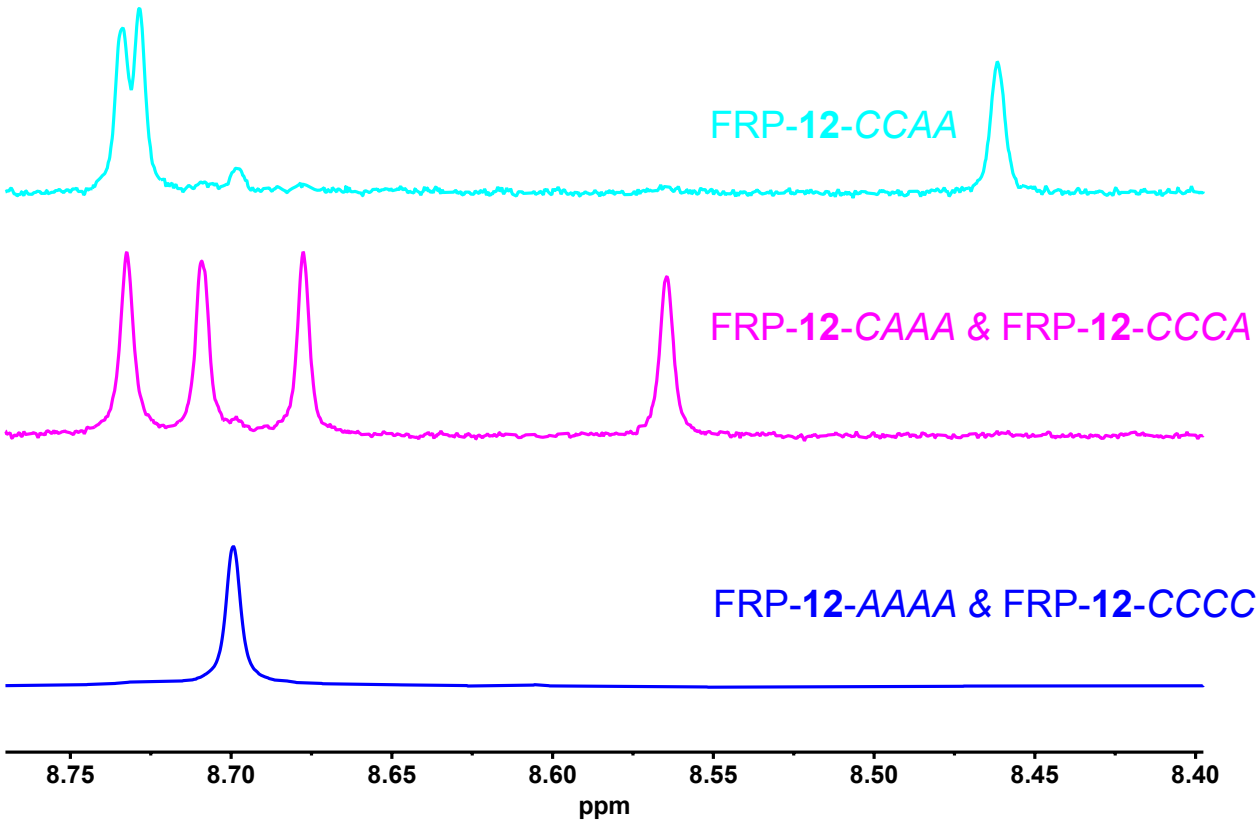

Figure S19 | Partial ^{1}H NMR spectrum of all diastereoisomers of FRP-**12**. FRP-**12**-*CCCC* and *AAAA* in *T*-symmetry exhibited only one signal for the protons in imine bonds (bottom), FRP-**12**-*CCCA* and *CAAA* in C_3-symmetry possessed four signals in the ratio of 1:1:1:1 for imine protons (middle) while FRP-**12**-*CCAA* in S_4-symmetry displayed three signals in the ratio of 1:1:1 for the H atoms in imine bonds (top).

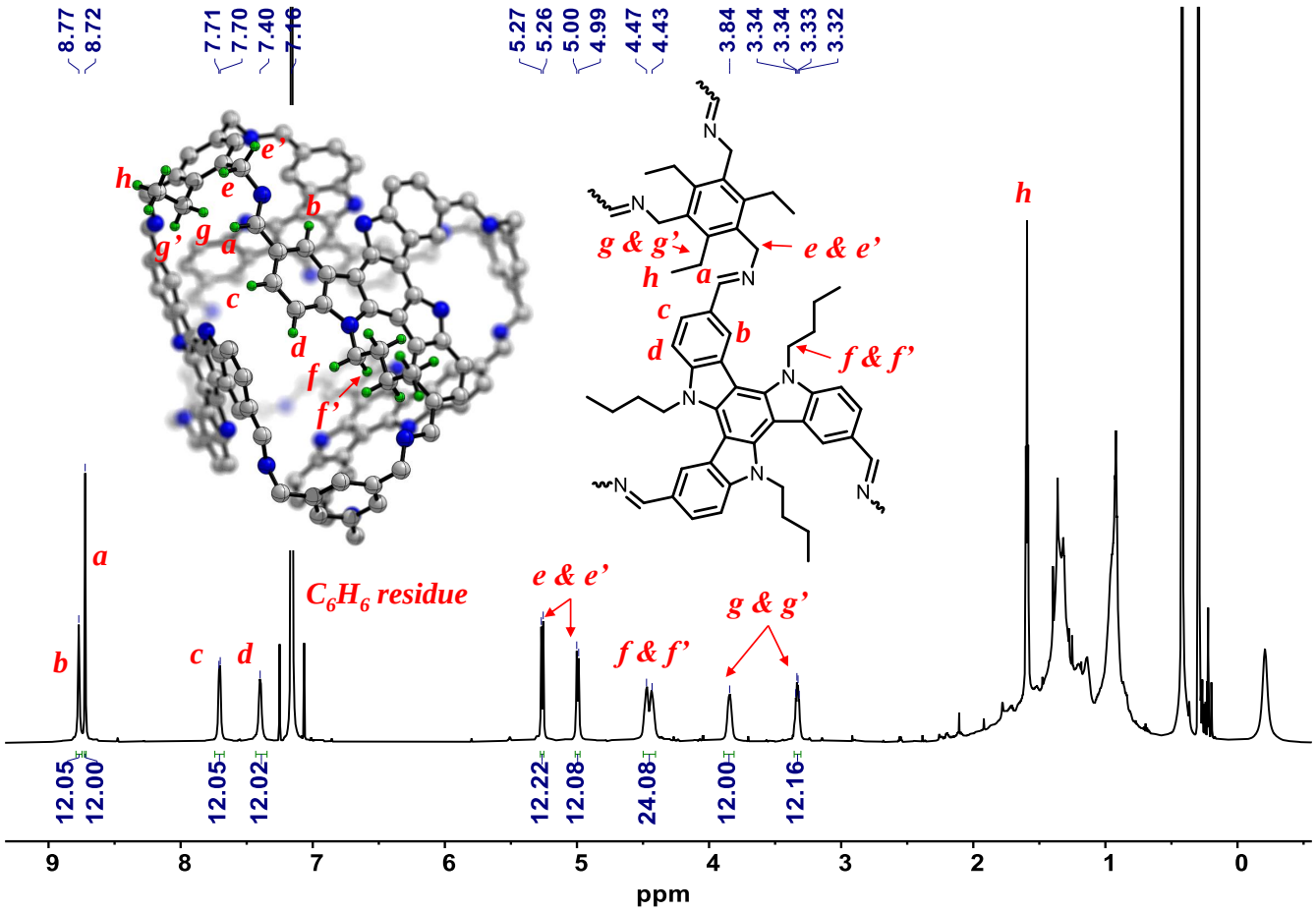

Figure S20 | ^{1}H NMR spectrum of FRP-**13**.

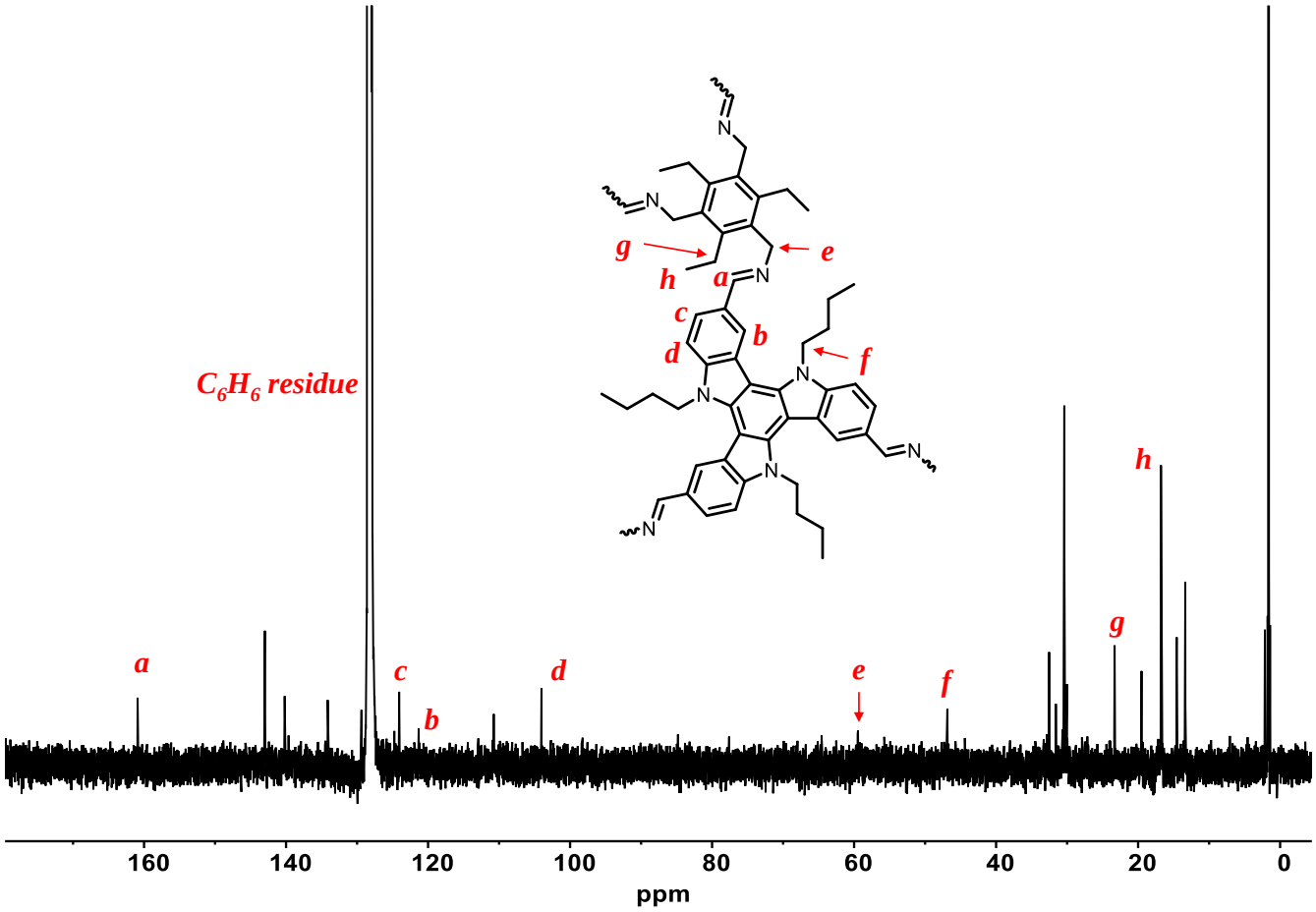

Figure S21 | ^{13}C NMR spectrum of FRP-**13**.

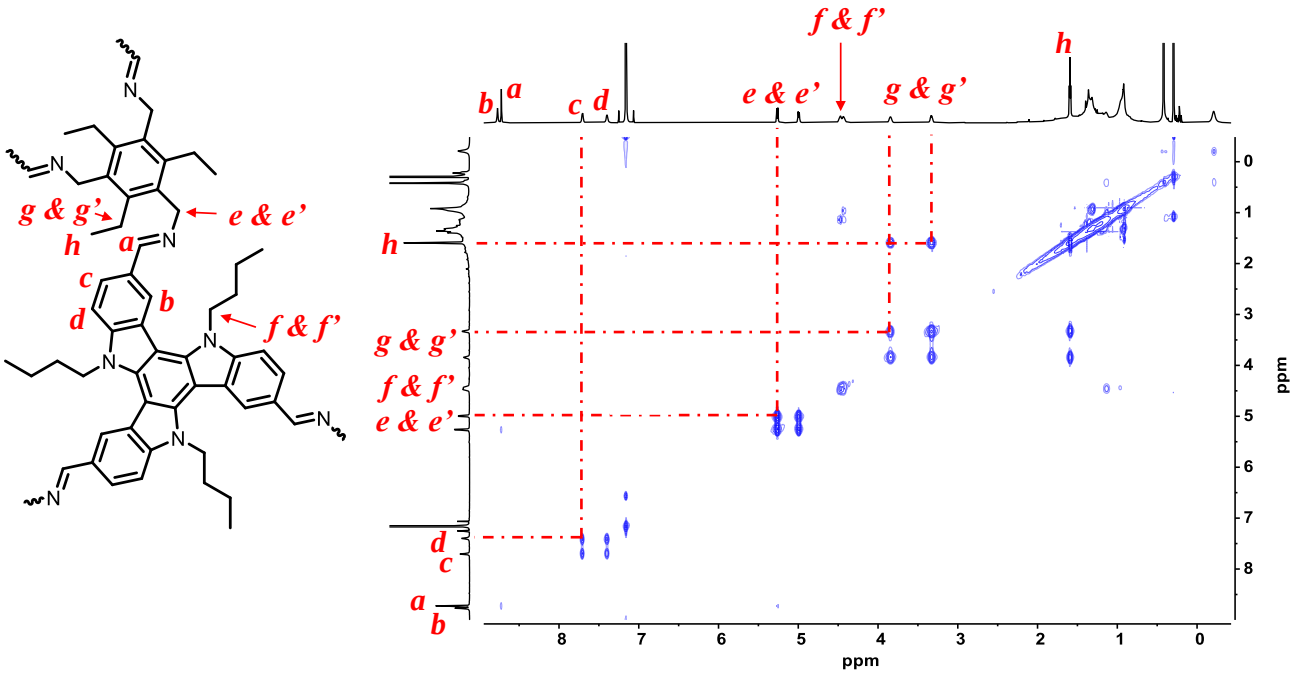

Figure S22 | H-H COSY spectrum of FRP-**13**.

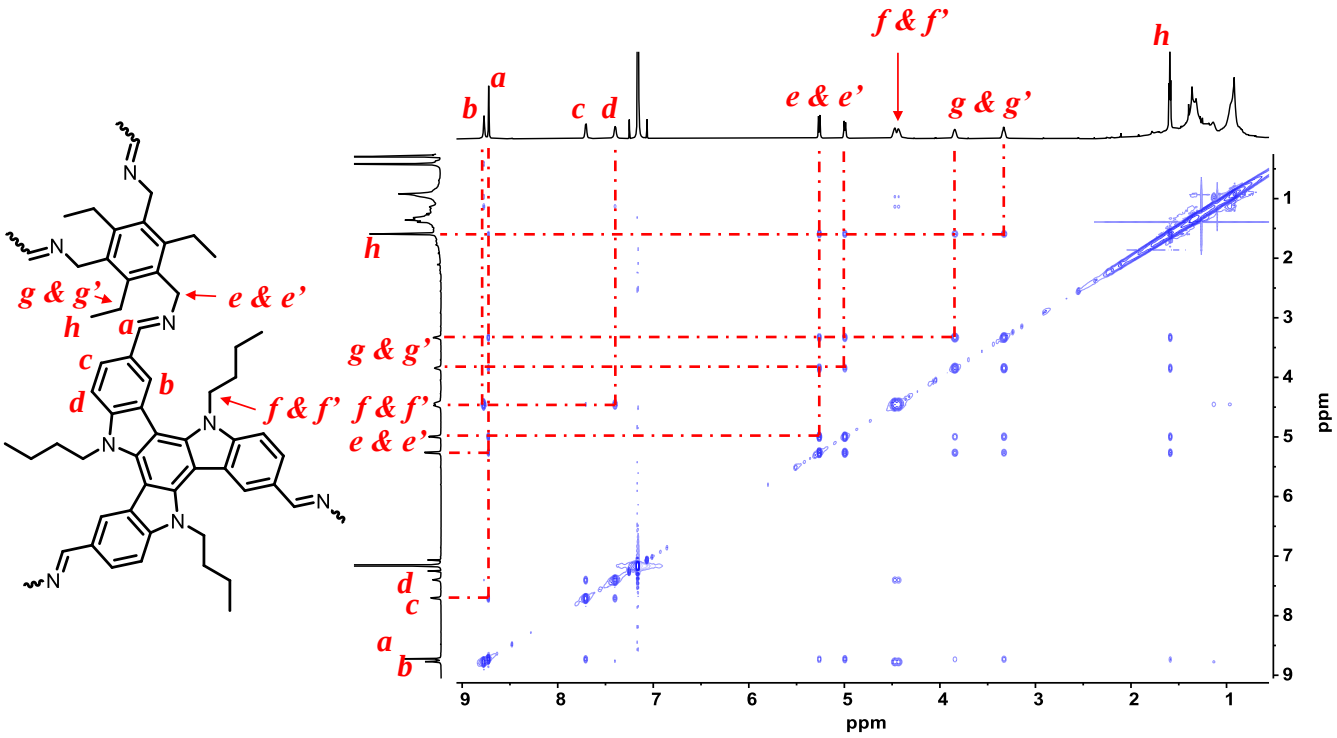

Figure S23 | NOESY spectrum of FRP-**13**.

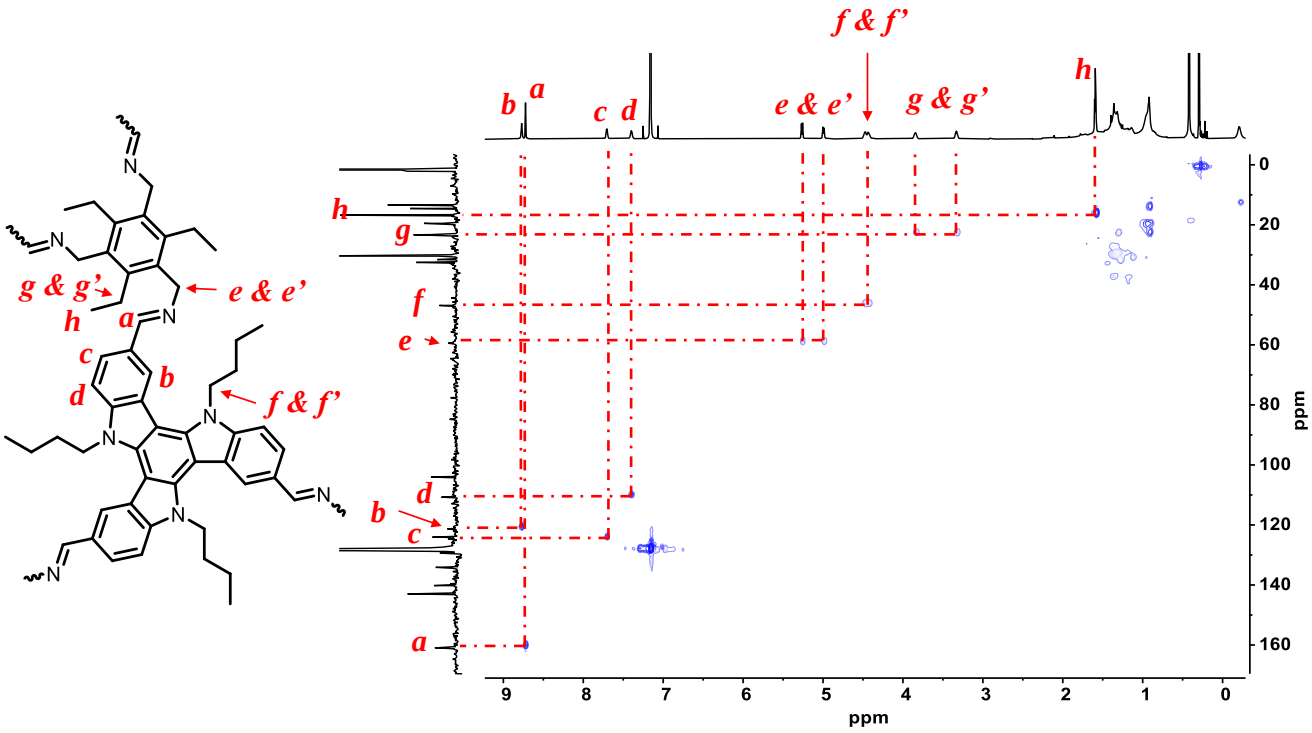

Figure S24 | HSQC spectrum of FRP-**13**.

4 HRMS spectra

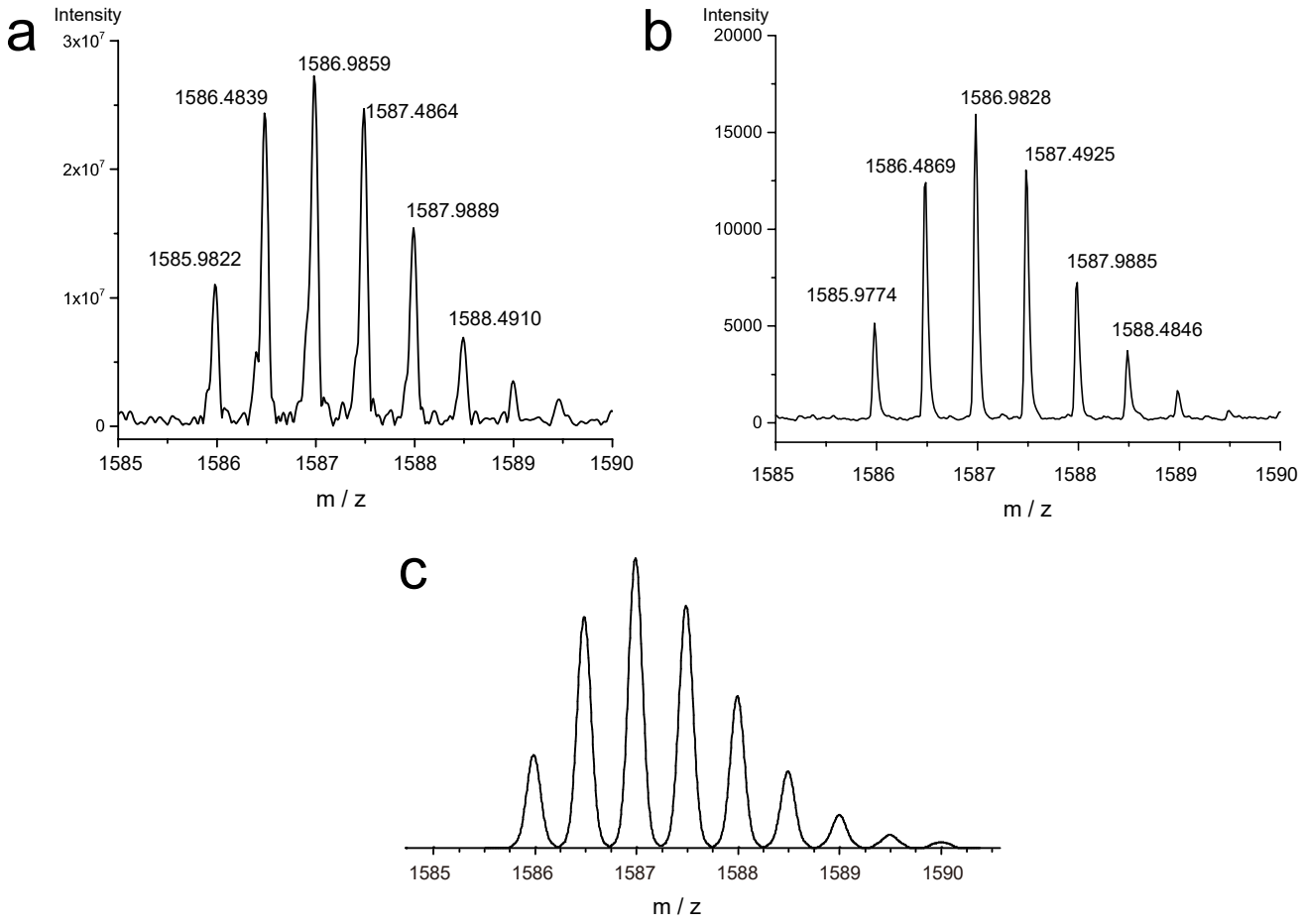

Figure S25 | HRMS spectrum of (a) FRP-**12** ($[M+2H]^{2+}$), (b) FRP-**13** ($[M+2H]^{2+}$) and (c) the calculated data.

5 Chiral HPLC analysis and CD spectra

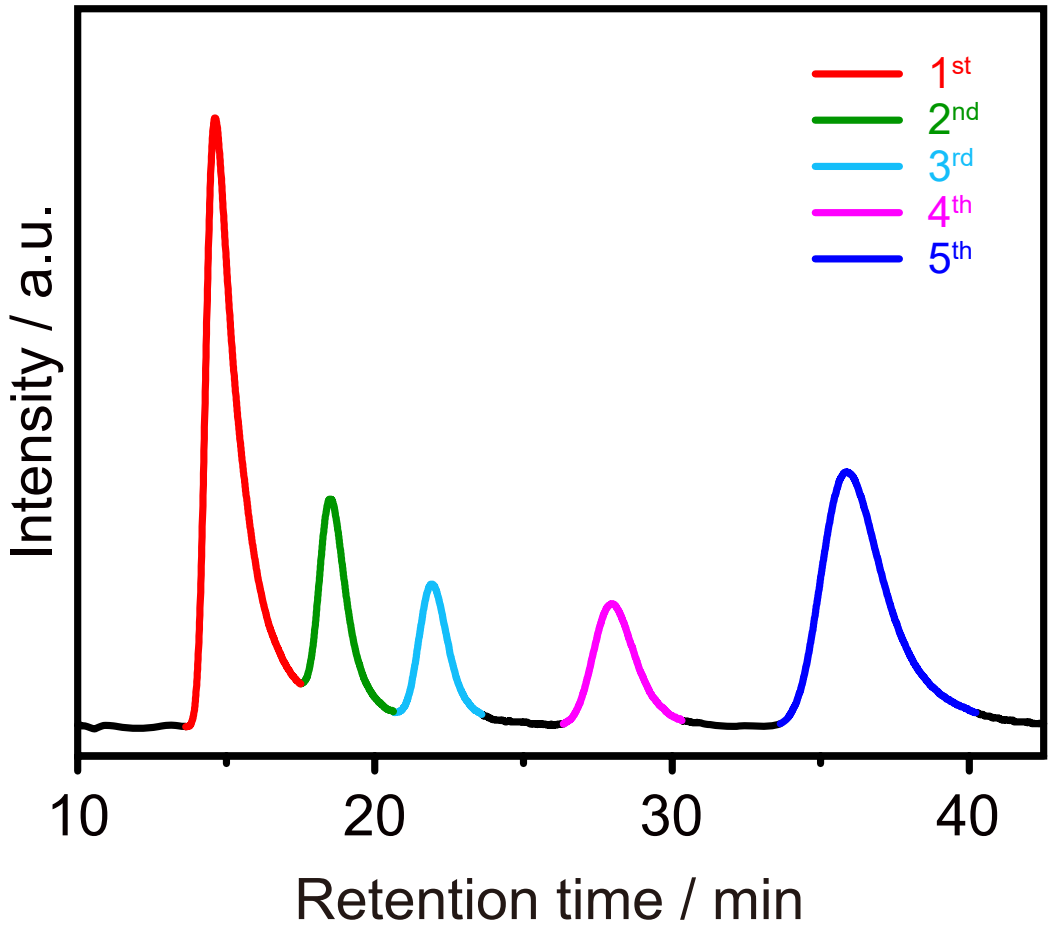

Figure S26 | Chiral HPLC analysis of FRP-**12**. The five components of FRP-**12** were separated by Daicel Chiralpak IE column and the mobile phase was consisted of hexane, toluene, methanol and chloroform in the ratio of 50 : 20 : 20 : 10.

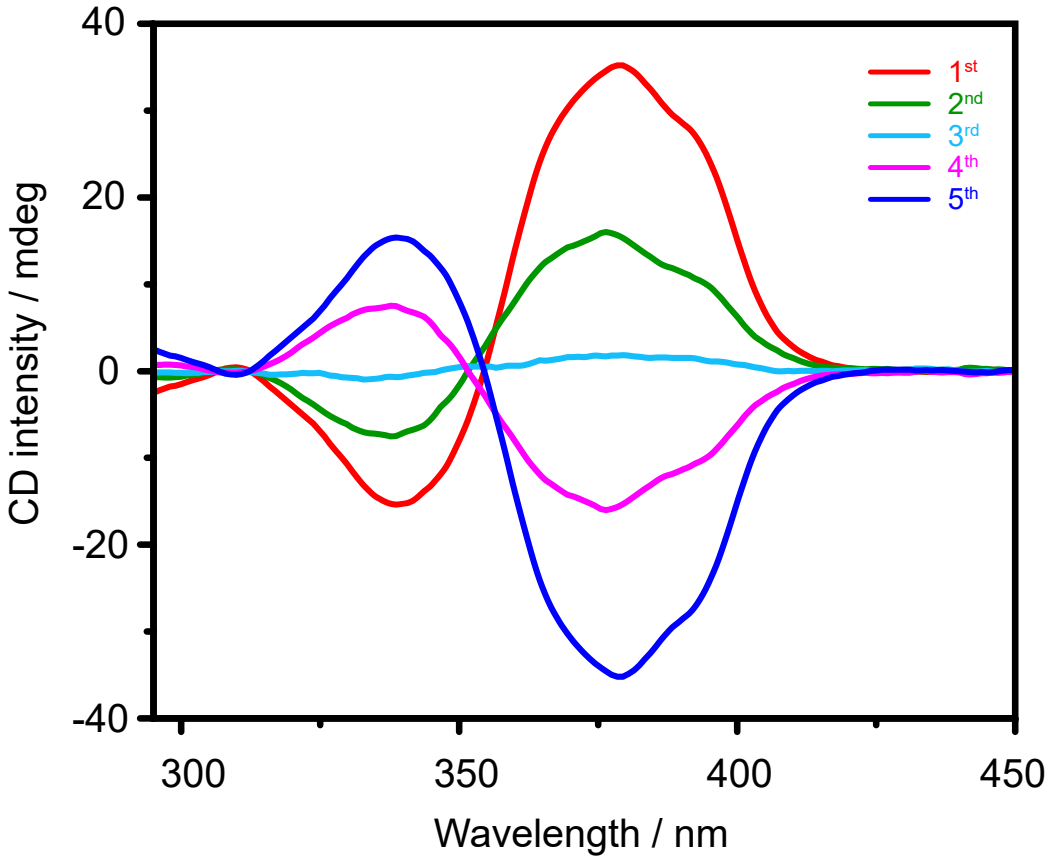

Figure S27 | CD spectrum of FRP-**12** performed in toluene.

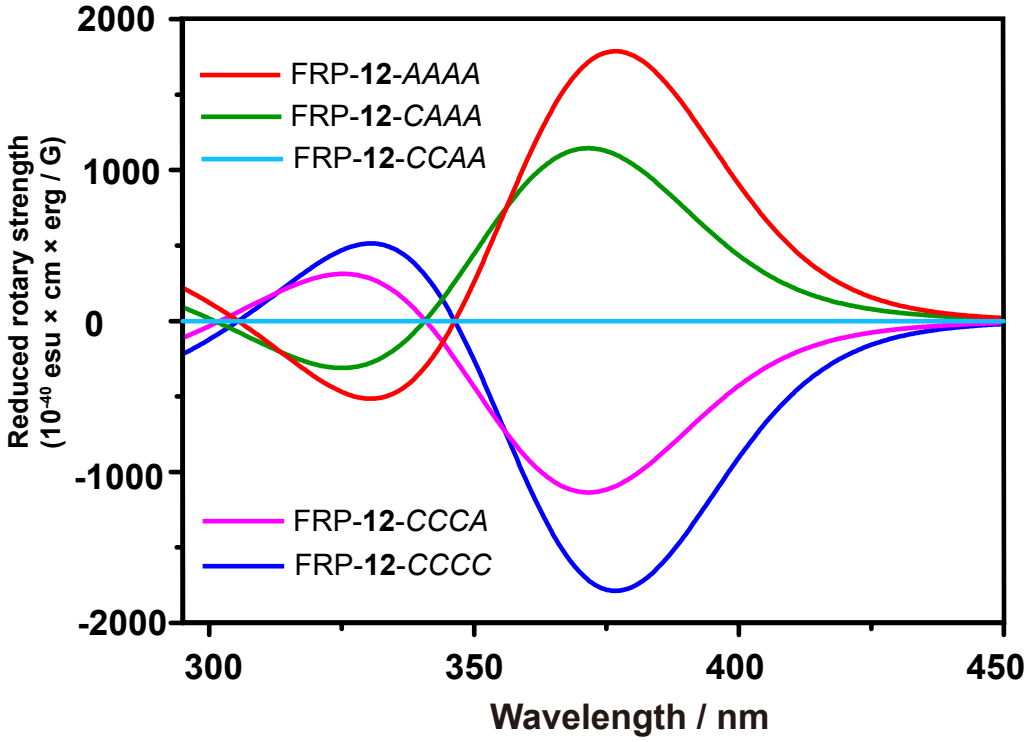

Figure S28 | Calculated CD spectrum of FRP-**12**.

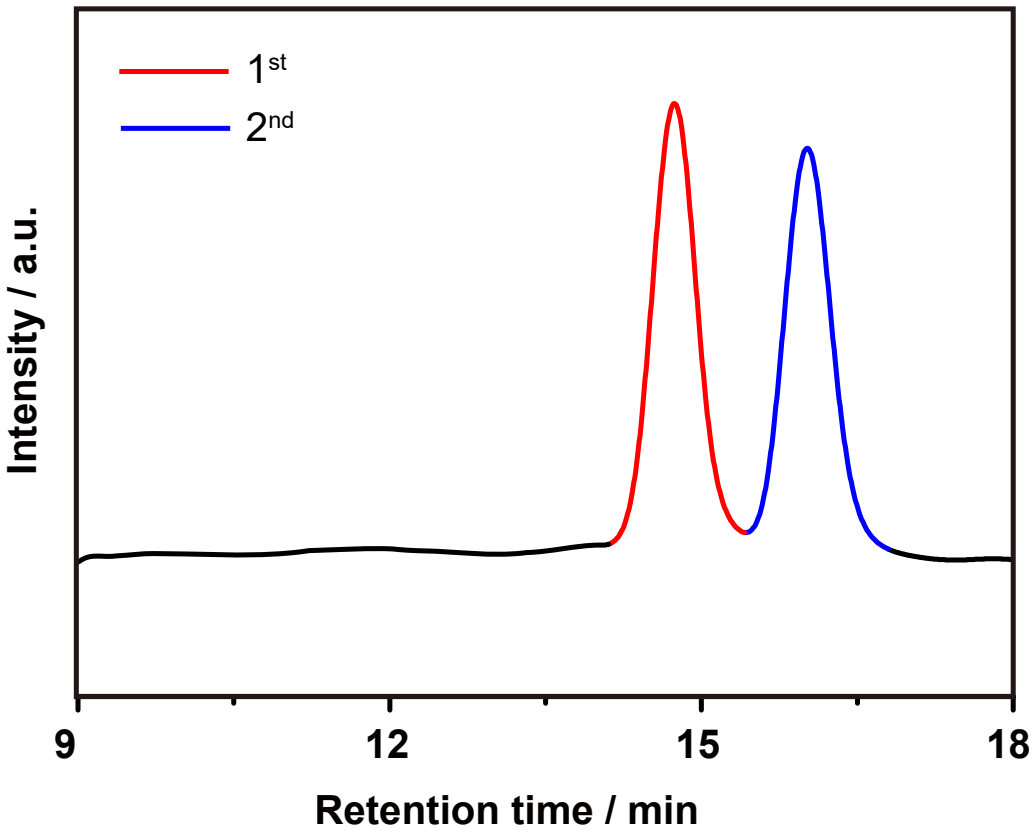

Figure S29 | Chiral HPLC analysis of FRP-**13**. The components of FRP-**13** were separated by Daicel Chiralpak IE column and the mobile phase was consisted of hexane, EA and chloroform in the ratio of 50 : 25 : 25.

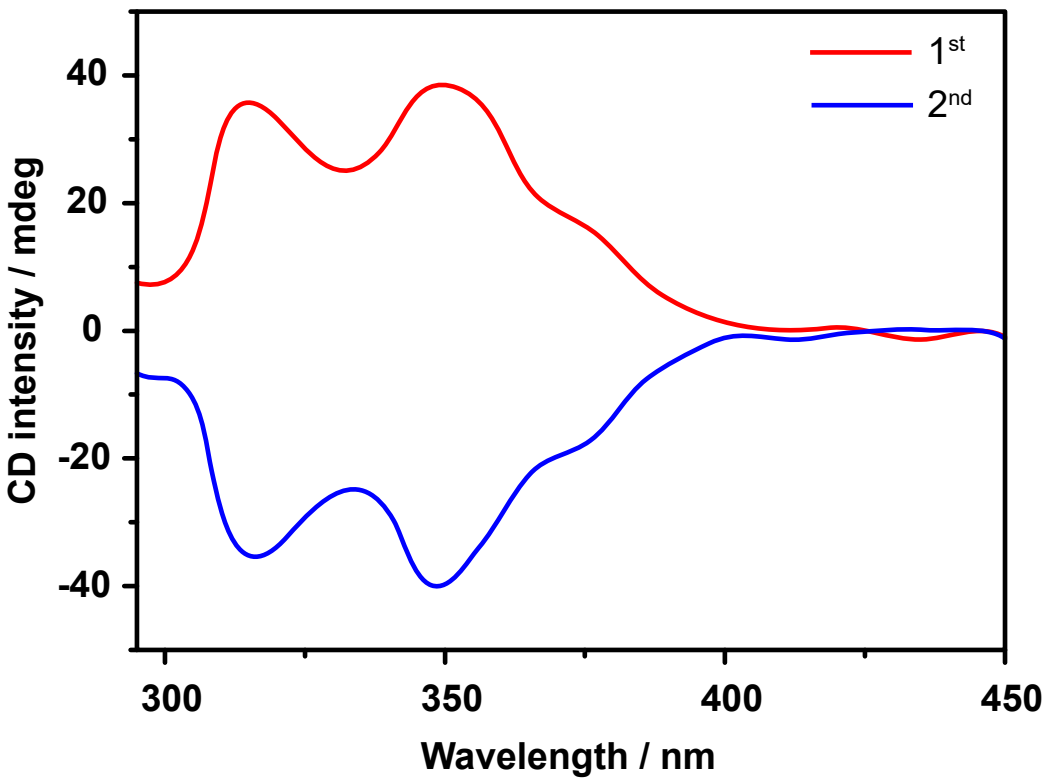

Figure S30 | CD spectrum of FRP-**13** performed in toluene.

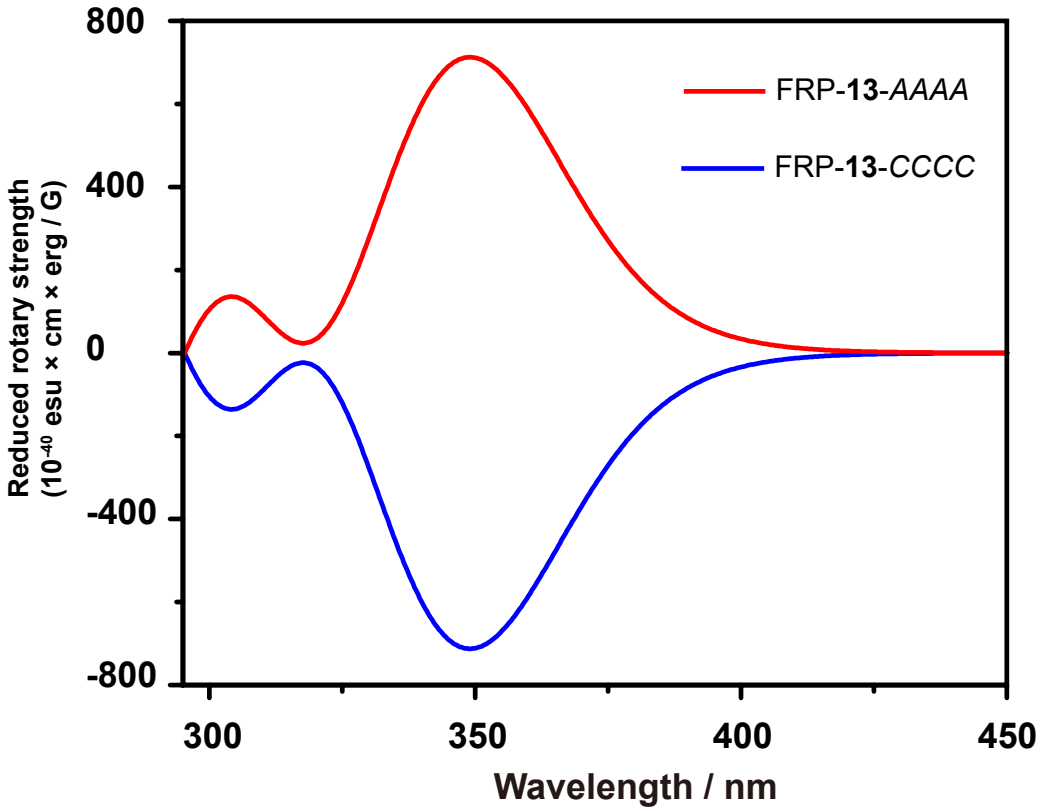

Figure S31 | Calculated CD spectrum of FRP-**13**. The difference between experimental and calculated spectrum can be attributed to deviation of ZINDO method. It is very difficult and expensive to calculate the excited state for FRP-**13**, which is a huge molecular system with 480 atoms. Although the ZINDO method exhibited poor accuracy on n-pi* transition, which is corresponded to the first peak in the CD spectra of FRP-**13**, it performed well on predicting the direction of Cotton effect for chiral molecular polyhedra.

6 Computational section

The ECD simulation was calculated using ZINDO method on Gaussian 16 used the optimized structures of FRP.

All the structural optimization and energy calculation were performed on Vienna Ab-initio Simulation Package (VASP, version 5.4.1), using gradient corrected (PBE) density functional theory in vacuum with D3-BJ dispersion Correction. The energy of FRP-**13**-*CCCA* and *CCAA* were 12.4 and 13.3 kcal/mol higher than that of FRP-**13**-*CCCC*, respectively. And the energy of FRP-**12**-*CCAA* and *CCCA* were 6.9 and 6.7 kcal/mol higher than that of FRP-**12**-*CCCC*, respectively. The energy calculation revealed the difference of stability between homo- and hetero-directional FRP, which was in consistent with the experimental results.

The diastereoselectivity of FRP-**13** was attributed to two types of repulsive interactions based on the DFT calculation. The first one is the repulsive forces among the butyl chains of hetero-directional **TAT** units, and the second type is the torsional strain of -C=N-C-C- bonds between **TAT** unit and **Tri-NH**$_2$ amine.

The repulsive interaction was well indicated by the reduced density gradient (RDG)[3] method. And the RDG analysis was performed on Multiwfn ver. 3.8[4]. The isosurface imagine was rendered by VMD ver 1.9.3[5].

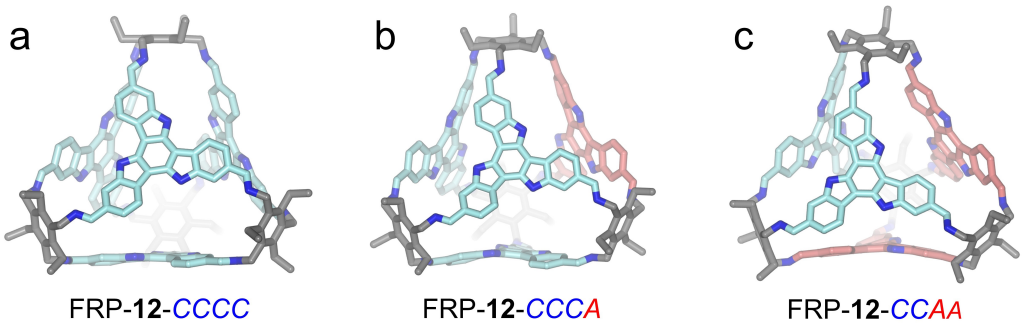

Figure S32 | Optimized Structures of FRP-**12** (a) *CCCC*, (b) *CCCA*, and (c) *CCAA*.

Repulsive interactions from butyl chains of TAT units:

In the optimized structure of FRP-**13**-*CCCA*, the butyl chains between *A*- and *C*-type of **TAT** units were very closed to each other, corresponding to the khaki area of EDG isosurface. On the other hand, the corresponded repulsive interaction in FRP-**12**-*CCCA* is much weaker than that in FRP-**13**.

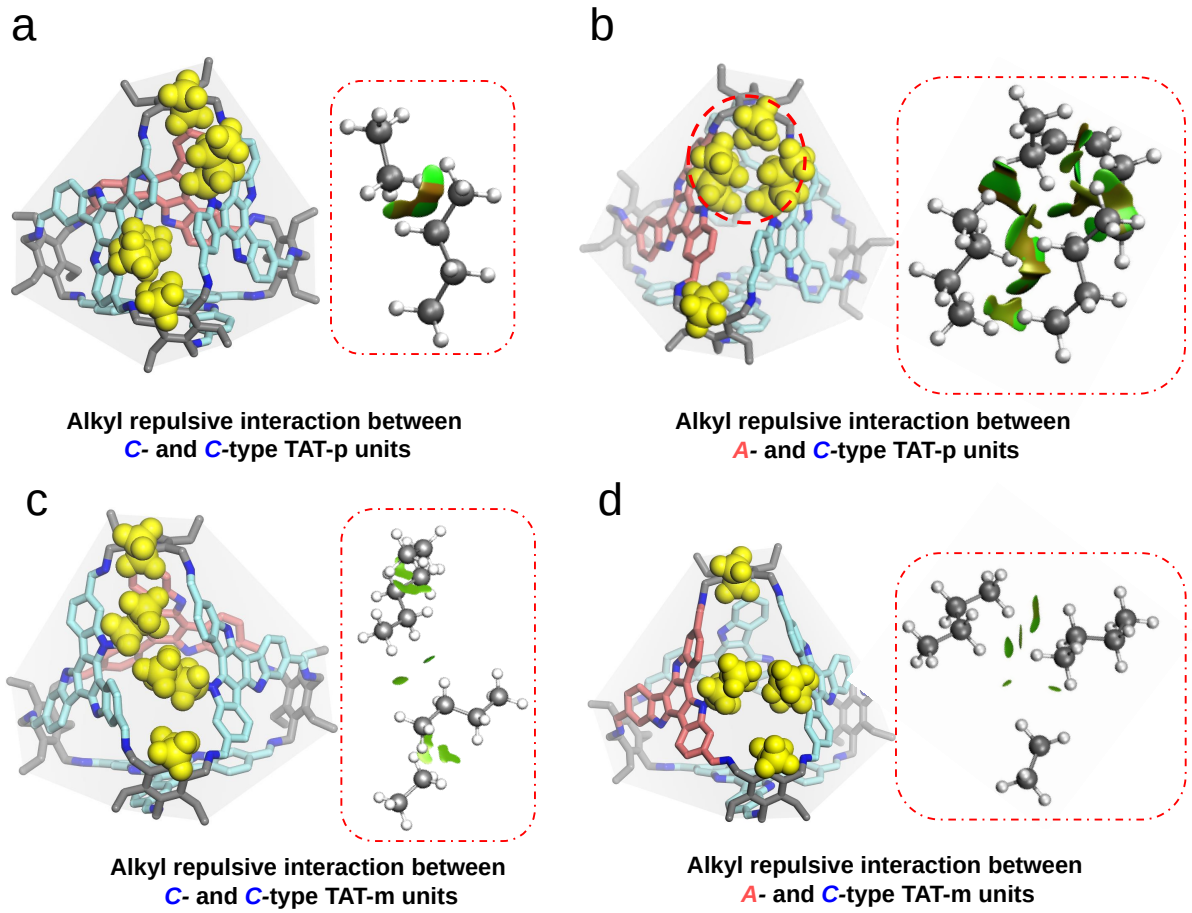

Figure S33 | Repulsive interactions from butyl chains and the corresponding RDG isosuface of **TAT** units in FRP-**13**-*CCCA* (a, b) and FRP-**12**-*CCCA* (c, d).

Repulsive interaction between the torsional imine bonds and Tri-NH_2: In the optimized structure of FRP-**13**-*CCCA*, the conformation of imine bonds was different in the *C*- and *A*-type **TAT**. The torsional conformation in *A*-type **TAT** brought strong repulsive forces among its imine proton and the atoms in **Tri-NH_2** amine, corresponding to the brown area of RDG isosurface.

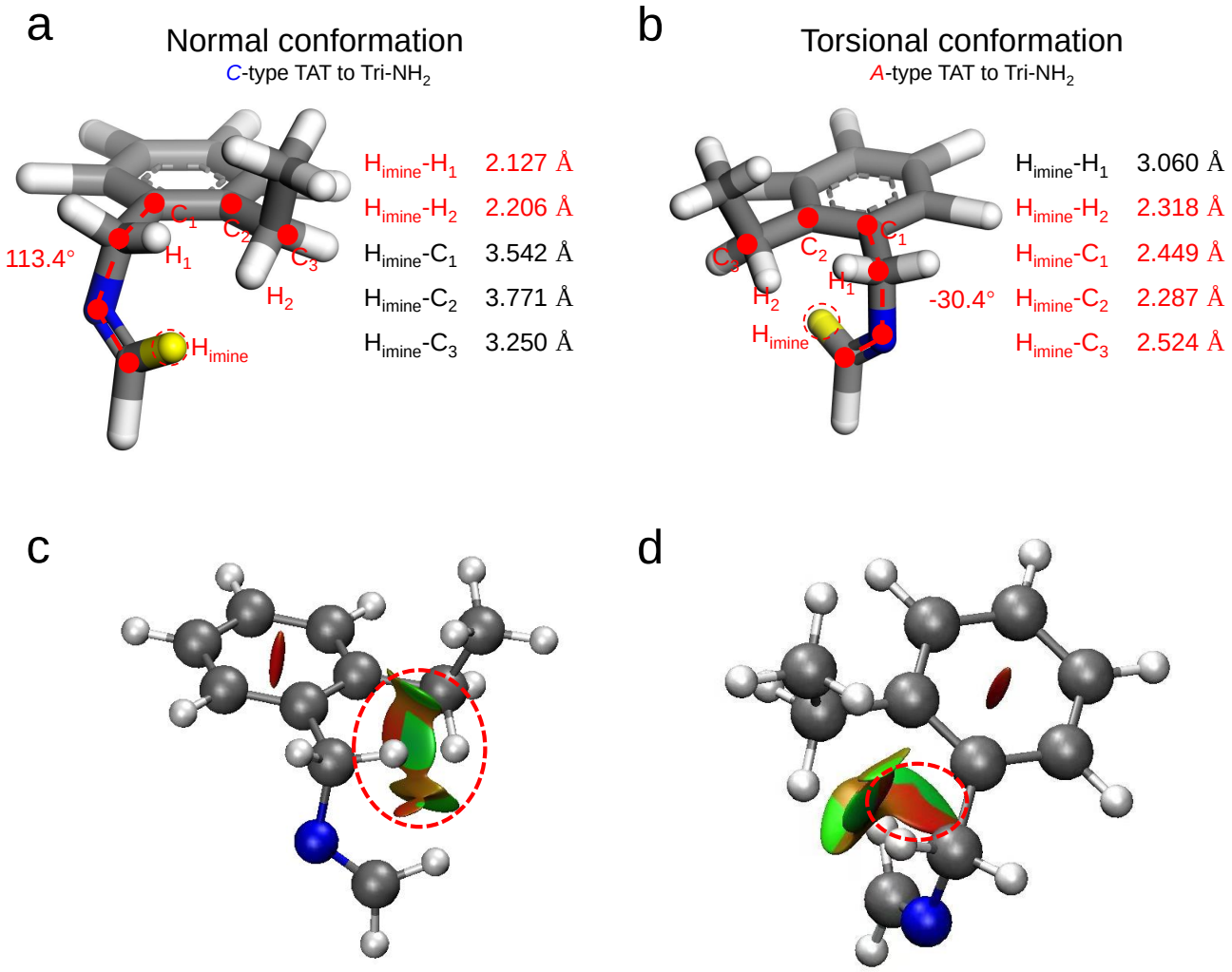

Figure S34 | For FRP-**13**-*CCCC*, the distance between imine proton and other atoms were listed in (a) and (b), illustrating that the imine proton in *A*-type **TAT** unit brought strong repulsive interaction to the FRP. In the RDG analysis, the brown area in (c) was the intrinsic repulsion between alkyl group, corresponding to the structure of *C*-type **TAT** unit and its adjacent **Tri-NH_2** units. But the brown area in (d) indicated the extra repulsive interaction between *A*-type **TAT** unit and its adjacent **Tri-NH_2** units.

In FRP-**12**, the second repulsive interaction is small enough to be ignored because of the stretched conformation of imine bonds in both *C*- and *A*-type **TAT** units.

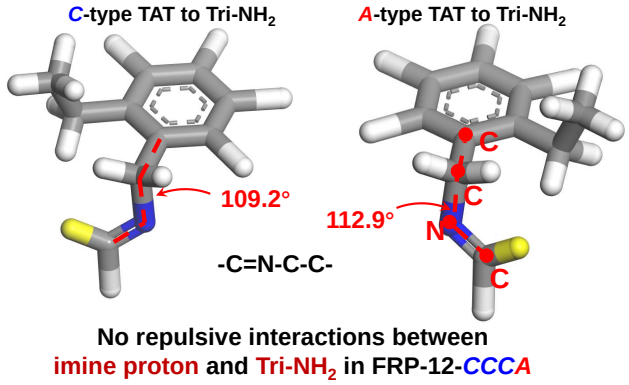

Figure S35 | Stretched conformation of imine bonds in *C*- or *A*-type **TAT** unit.

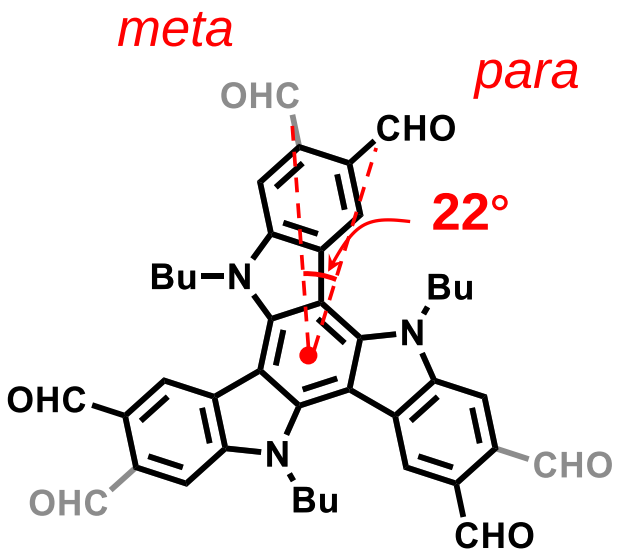

Figure S36 | Changing the formyl linking group from *meta*-substituted (**TAT-m**) to *para*-substituted (**TAT-p**), the **TAT** units rotated about 22° in the faces of [4+4] molecular polyhedra and resulted in distinct spatial arrangement of the butyl groups and imine bonds.

7 Single crystal data

Crystal growing:

The crystals of FRP-**13** suitable for X-ray analysis were grown by diffusing methanol (3 mL) into saturated toluene solution of FRP-**13** (1.5 mL). Transparent hexagonal prisms crystals appeared after two months. Single crystal X-ray diffraction data were collected on Rigaku SuperNova X-Ray single crystal diffractometer using Cu K_α (λ = 1.54184 Å) micro-focus X-ray sources. Suitable crystal was collected, covered with protective oil and mounted on X-ray diffractometer. FRP-**13** contain only light elements (i.e., C, H, and N). The crystal was kept in 100 K with liquid nitrogen stream during the unit cell determination and full data collection. The raw data were collected and reduced by CrysAlisPro software, the structures were solved with the SHELXS[6] or SHELXT[6] using Direct Methods and refined with the SHELXL[6] using CGLS minimization, and OLEX2[7] were used as GUI.

Refinement details:

For crystal of FRP-**13**, all non-hydrogen atoms were refined anisotropically. Hydrogen atoms were placed at calculated positions using the riding model and refined isotropically. The instructions AFIX 23 and AFIX 43 were used for the hydrogen atoms on the secondary -CH_2- and the aromatic C-H, respectively, with the parameter of U_{iso}=1.2 U_{eq}. The instruction AFIX 33 was used for the hydrogen atoms on the highly disordered terminal -CH_3 groups with the parameter of U_{iso}=1.5 U_{eq}. No Shelx restraint was applied to the skeleton of the molecular prism, i.e. triazatruxene faces and **Tri-NH$_2$** units. Nevertheless, butyl groups outside the cage are expected to be highly disordered, as they are flexible and would vibrate randomly in the large voids in the crystal. Therefore, necessary Shelx restraints (i.e., DELU, SIMU, and EADP) were applied to the butyl groups to result in a reasonable model. Specifically, the anisotropic displacement parameters of disordered atoms in butyl groups were restrained to be equal within an effective standard deviation of 0.01 using the DELU command. U_{ij} values of disordered atoms of butyl groups were constrained to be similar using the SIMU command. Atomic displacement parameters (ADPs) of different parts of disordered atoms were restrained using the EADP command. Only the homo-directional FRP were found in the crystal structure. And the FRP-**13**-*AAAA* and its mirror image, FRP-**13**-*CCCC*, were packed in $R\bar{3}c$ space group. The orientation of imide bonds is depended on the rotational patterns of **TAT** facial building blocks.

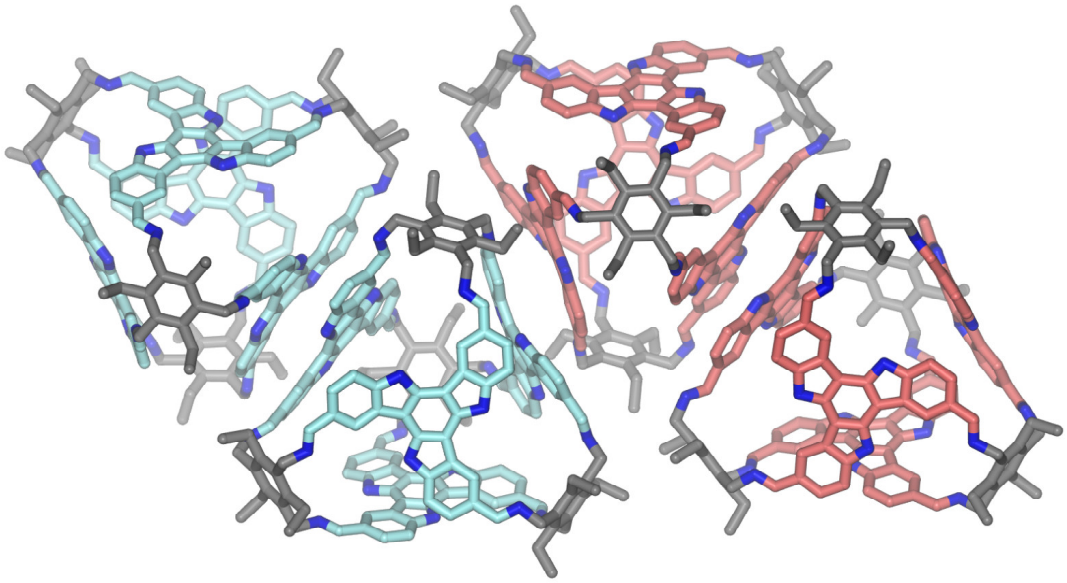

Figure S37 | Single-crystal XRD analysis of FRP-**13** revealed that a pair of tetrahedral enantiomers (*AAAA* and *CCCC*) were crystalized in $R\bar{3}c$ space group. **TAT** facial units shifts closer to the centroid of the cage for efficient packing between the homo-directional tetrahedra (*CCCC* and *CCCC*, or *AAAA* and *AAAA*). Hydrogen atoms and partial alkyl chains were omitted for clarity.

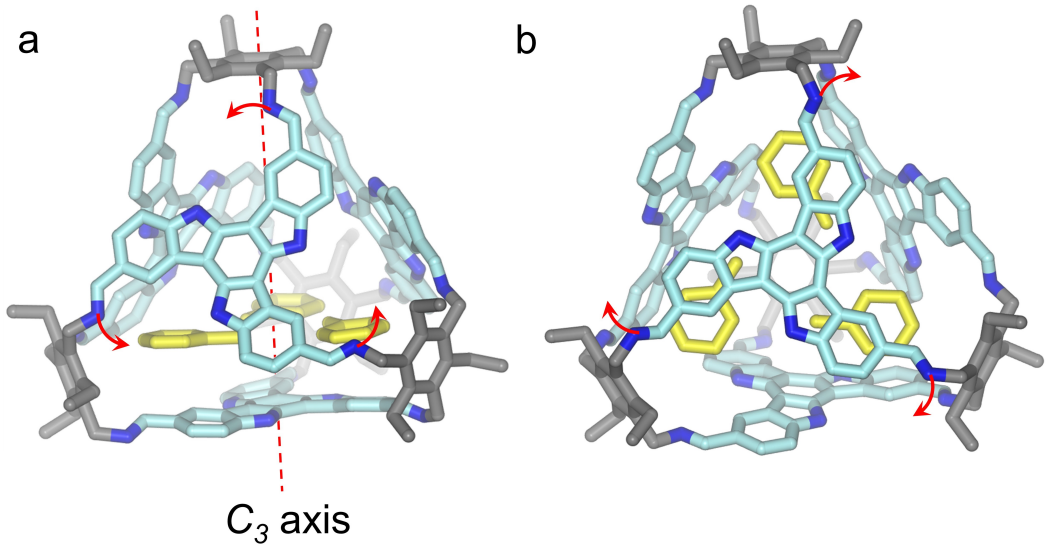

Figure S38 | (a) Front and (b) bottom side of the crystal structure of FRP-**13**-*CCCC*. In the crystal structure, one of the **TAT** facial units shifts closer to the centroid of the cage, making the solid-state confor-mation of FRP-**13** C_3-symmetric.

Table S1: Crystal data and structure refinement for FRP-**13**

CCDC	2053589
Identification code	FRP-13
Empirical formula	$C_{237}H_{264}N_{24}$
Formula weight	3448.74
Temperature/K	100.01(10)
Crystal system	trigonal
Space group	$R\bar{3}c$
a/Å	27.801(2)
b/Å	27.801(2)
c/Å	100.433(8)
α/°	90
β/°	90
γ/°	120
Volume/Å^3	67223(11)
Z	11.99988
ρ_{calc}g/cm^3	1.022
μ/mm^{-1}	0.458
F(000)	22248.0
Crystal size/mm^3	$0.2 \times 0.1 \times 0.1$
Radiation	CuKα (λ = 1.54184)
2Θ range for data collection/°	5.28 to 139.164
Index ranges	$-33 \leq h \leq 31$, $-32 \leq k \leq 31$, $-113 \leq l \leq 120$
Reflections collected	135827
Independent reflections	12999 [R_{int} = 0.1365, R_{sigma} = 0.0655]
Data/restraints/parameters	12999/0/807
Goodness-of-fit on F^2	1.102
Final R indexes [$I>2\sigma$ (I)]	R_1 = 0.1055, wR_2 = 0.3154
Final R indexes [all data]	R_1 = 0.1607, wR_2 = 0.3751
Largest diff. peak/hole / e Å^{-3}	0.50/-0.32

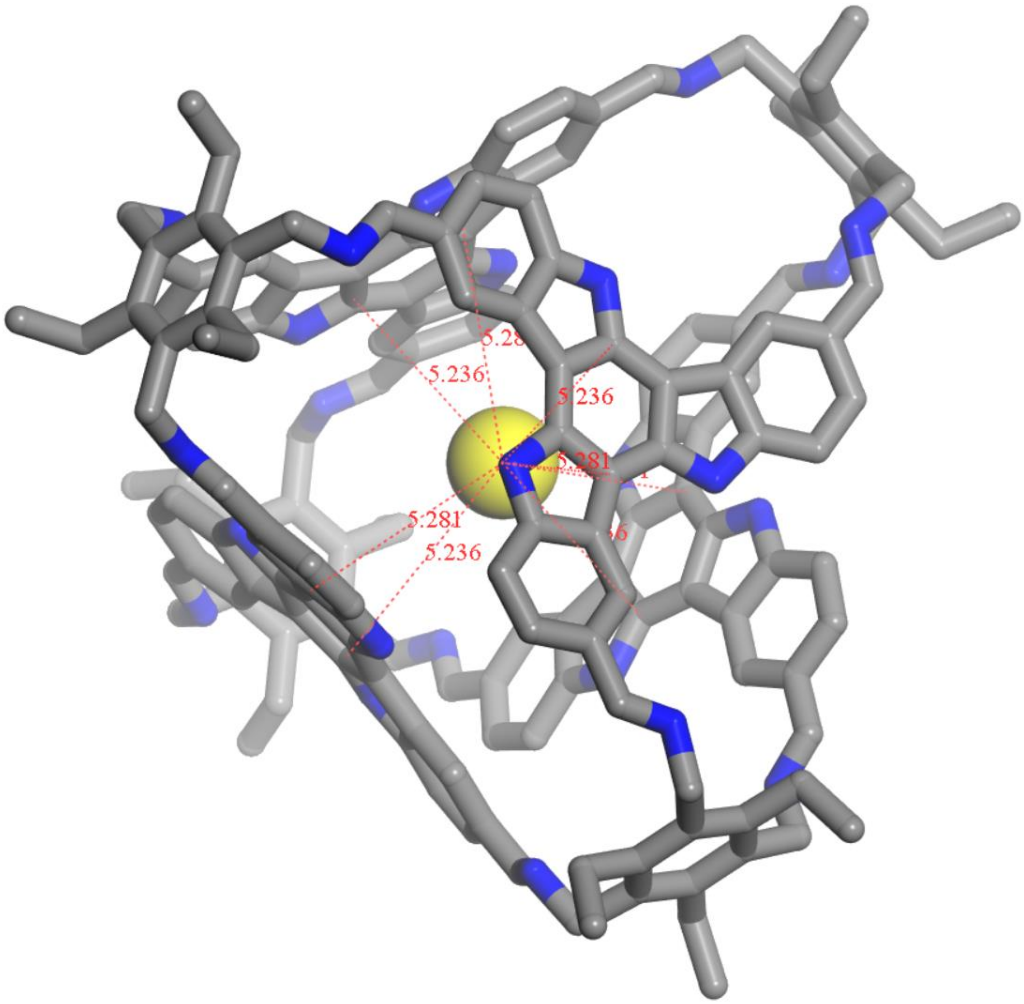

Figure S39 | The cavity of FRP-**13**-*CCCC* was calculated to be 609 Å^3 according to the radius of its inscribed sphere. And the radius was measured to be 5.26 Å. Hydrogen atoms and partial alkyl chains were omitted for clarity.

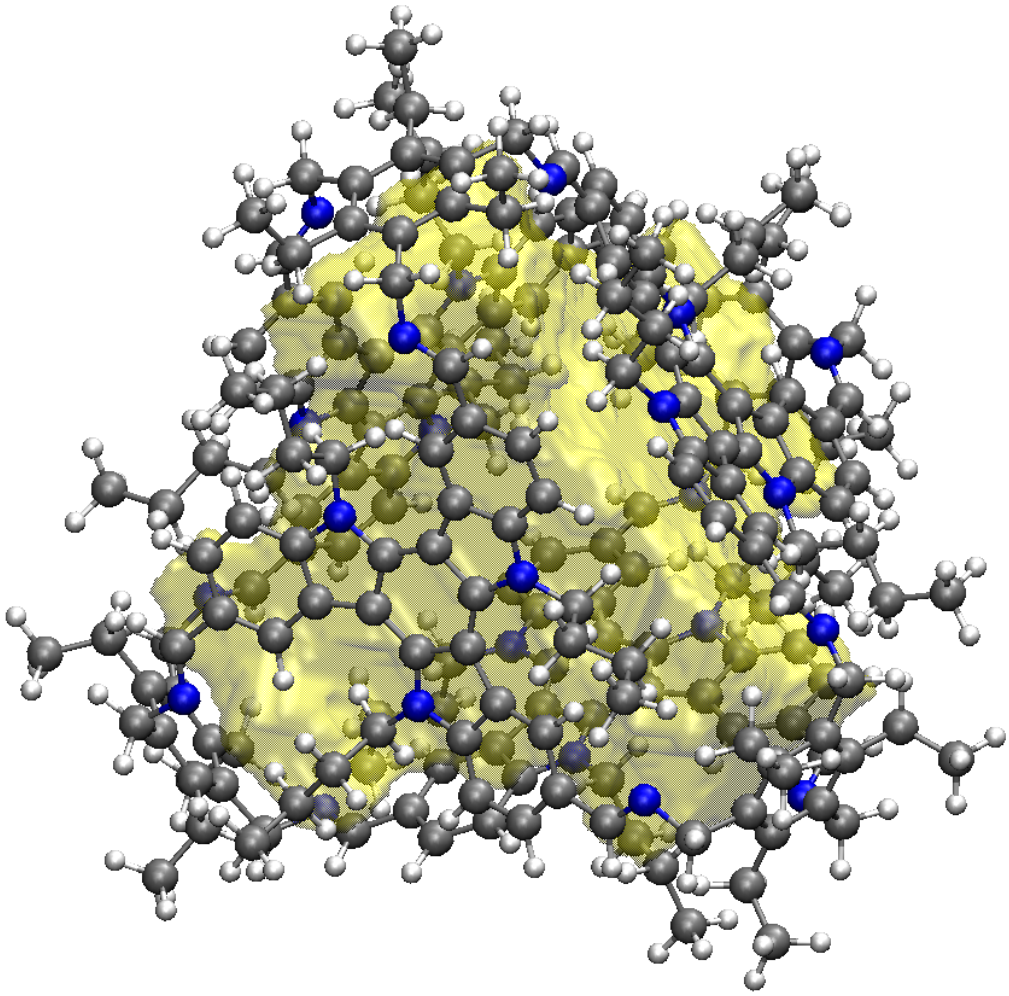

Figure S40 | The volume of cavity in FRP-**13**-*CCCC*/*AAAA* was integrate to be 772 Å^3 by promolecular density. The calculation was performed on Multiwfn Ver. 3.8[4] and the isosurface imagine was rendered by VMD ver. 1.9.3.[5]

References

[1] Zhang, P.; Wang, X.; Xuan, W.; Peng, P.; Li, Z.; Lu, R.; Wu, S.; Tian, Z.; Cao, X. *Chem. Commun.* **2018**, *54*, 4685–4688.

[2] Lauer, J. C.; Zhang, W.-S.; Rominger, F.; Schröder, R. R.; Mastalerz, M. *Chem. Eur. J.* **2018**, *24*, 1816–1820.

[3] Johnson, E. R.; Keinan, S.; Mori-Sánchez, P.; Contreras-Garcła, J.; Cohen, A. J.; Yang, W. *J. Am. Chem. Soc.* **2010**, *132*, 6498–6506.

[4] Lu, T.; Chen, F. *J. Comput. Chem.* **2012**, *33*, 580–592.

[5] Humphrey, W.; Dalke, A.; Schulten, K. *J. Mol. Graphics* **1996**, *14*, 33–38.

[6] Sheldrick, G. M. *Acta Cryst. Sect. C* **2015**, *71*, 3–8.

[7] Dolomanov, O. V.; Bourhis, L. J.; Gildea, R. J.; Howard, J. A. K.; Puschmann, H. *J. Appl. Crystallogr.* **2009**, *42*, 339–341.